CHALMERS
UNIVERSITY OF TECHNOLOGY

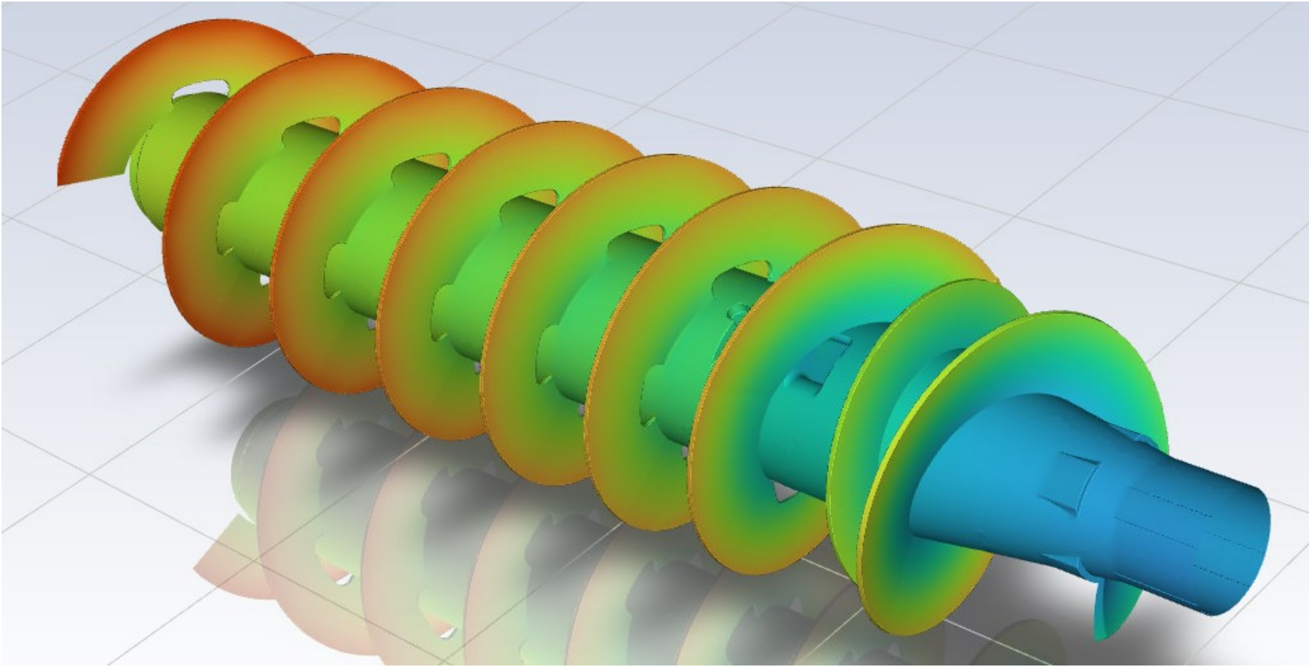

Analysis of Multiphase Flow Centrifuge Decanter Separator Using CFD Simulations

Master's thesis in Innovative and Sustainable Chemical Engineering

AHMED KHOGALI

DEPARTMENT OF CHEMISTRY AND CHEMICAL ENGINEERING

CHALMERS UNIVERSITY OF TECHNOLOGY
Gothenburg, Sweden 2022
www.chalmers.se

Master's thesis 2022

Analysis of Multiphase Flow Centrifuge Decanter Separator Using CFD Simulations

AHMED KHOGALI

Department of Chemistry and Chemical Engineering
Chalmers University of Technology
Gothenburg, Sweden 2022

Analysis of Multiphase Flow Centrifuge Decanter Separator Using CFD Simulations
AHMED KHOGALI

Supervisors:
Jonas Bredberg, PhD., Technical Account Manager, EDR&Medeso
Hector Forero-Hernandez, PhD., CFD and Test Engineer, Alfa Laval

Examiner: Ronnie Andersson, Professor, Department of Chemistry and Chemical Engineering, Chalmers University of Technology

Master's Thesis 2022
Department of Chemistry and Chemical Engineering
Chalmers University of Technology
SE-412 96 Gothenburg
Telephone +46 31 772 1000

Cover: Decanter Separator. Contour of static pressure in the conveyor by Ahmed Khogali.

Typeset in LaTeX
Printed by Chalmers Reproservice
Gothenburg, Sweden 2022

Analysis of Multiphase Flow Centrifuge Decanter Separator Using CFD Simulations
AHMED KHOGALI
Department of Chemistry and Chemical Engineering
Chalmers University of Technology

Abstract

In the industry, it is common to encounter multiphase flow in many different applications in the oil and gas, food production and waste treatment industries. The nature of multiphase flow is extremely complex and is continuously developing in terms of methods and tools to perform analysis. One device in the industry involving mutiphase flow is the centrifuge decanter separator for sewage water treatment with the aim of separating fluid and solids. The centrifuge decanter in this study is a separator from Alfa Laval (AL). This study aims at analyzing the decanter by using computational fluid dynamics (CFD) as a simulation tool in combination with the field of multiphase flow modeling to understand the decanter's different components and complex functions at high rotational speeds. This makes the decanter a very demanding topic for this type of research. The analysis of the phenomena was done through systematic changes in parameters, strategies and models. The Euler-Euler and Mixture multiphase models were used to predict the distribution of water and solids throughout the domain within the decanter separator and determine how efficient the separation process is in terms of the amount of exiting solids. Operation parameters such as the differential speed of the decanter parts and boundary conditions within the domain were analyzed and results were presented.

Keywords: CFD, Computational Fluid Dynamics, Multiphase, Decanter, Separator, Mixture Model, Euler-Euler, Simulation, ANSYS, Fluent.

Acknowledgements

During my time at Chalmers, I have been fortunate to meet many people that have inspired me. People that have helped me. People that I would struggle together with and celebrate alongside. The global pandemic over the last couple of years have made studies unusual in many aspects. That combined with moving and adapting to a new culture and environment has made this challenging but ultimately a very rewarding experience that has helped me grow as a person.

This thesis work would not have been possible without the help of my supervisors. I would like to express my sincere gratitude to Dr. Jonas Bredberg for his continuous support, patience, constant guidance and for given me this amazing opportunity. I would like to extend my many thanks to Dr. Hector Forero-Hernandez for all the support he has given me, his insightful comments and ideas and for answering my many questions. Also, I would like to thank Prof. Ronnie Anderson for his willingness to take on the role as an examiner for this thesis and for his support throughout this project. My thanks go out to everyone at EDR&Medeso for their unending kindness and understanding. Special thanks to Tony Eriksson, Klas Johansson, Tomas Jarneholt and Henrik Tryggeson for their help at different stages of this work.

Lastly, I want to give my endless gratitude to my father, mother, brother and sister. Thank you for always believing in me and supporting my decisions. I am forever grateful.

Ahmed Khogali, Gothenburg, June 2022

List of Acronyms

Below is the list of acronyms that have been used throughout this thesis listed in alphabetical order:

CFD	Computational Fluid Dynamics
DNS	Direct Numerical Simulations
LES	Large Eddy Simulations
RANS	Reynolds Averaged Navier Stokes
RSM	Reynolds Stress Model
SIMPLE	Semi-Implicit Method for Pressure-Linked Equations
SST	Shear Stress Transport
VOF	Volume of Fluid

Nomenclature

Below is the key nomenclature of symbols that have been used throughout this thesis.

Latin Symbols

A	Area, m^2
Cr	Friction Coefficient Between Particles, -
D	Diameter, m
e	Restitution Coefficient, -
F	Force, N
g	Gravity, m/s^2
g_0	Radial Distribution Function, -
G	Distance Between Two Consecutive Blade Edges, m
h	Enthalpy, kJ
I_{2D}	Principle Strain Rate Tensor, 1/s
j	Diffusional Flux, $mol/m^2 s$
k	Turbulent Kinetic Energy, m^2/s^2
K	Momentum Exchange Coefficient, -
L	Length, m
m	Mass, kg
$\dot{m}$	Mass Flow Rate, kg/s
p_d	Total Particle Pressure, kg/m
P	Pressure, Pa
r_o	Inner Radius of the Bowl, m
Re	Reynolds Number, -
S	Source Term
St	Stokes Number, -

t	Time, s
T	Temperature, K
U	Velocity, m/s
V	Volume, m^3
y^+	Dimensionless Distance From Wall, -

Greek Symbols

α	Volume Fraction, -
Δ	Rotational Speed Difference, rpm
ϵ	Turbulent Dissipation Rate, m^2/s^3
η	Angle of Internal Friction, Degrees
θ	Granular Temperature, m^2/s^2
μ	Dynamic Viscosity, kg/m.s
μ_d	Granular Viscosity, kg/m.s
ν	Kinematic Viscosity, $\mathrm{m/s}^2$
ρ	Density, $\mathrm{kg/m}^3$
τ	Viscous Stress Tensor, $\mathrm{N/m}^2$
ω	Turbulent Specific Dissipation Rate, 1/s

Contents

1
Introduction

The increasing demand for improving devices in the industry over the last few years has made it necessary to design and manufacture highly efficient and technologically advanced devices and units. A decanter centrifuge is a separator device that uses a combination of density differences and centrifugal forces to separate mixtures containing solids and liquids. On the surface, it might appear as a complicated piece of machinery but the decanter uses a simple principle, the use of a screw conveyor located within a cylindrical bowl both rotating at high speeds. The conveying motion driving the separation of phases is a result of the slightly different rotational speeds between the conveyor and bowl. This difference in rotational speed creates a centrifugal force and thus helps in the separation. A decanter is made from several other parts including a gearbox, feed zone, feed tube, a bowl and also inlet and outlet discharge openings. A decanter also uses flow conditions such as vanes and blades and other chemical additives such as polymers to enhance the separation.

Many of the applications in the industry include the analysis of flow fields and the majority of flows include multiphase. Multiphase flow modeling can be defined as the use of simulation tools to study multiple phases through the analysis of mass, momentum and energy transfer of a flow field. There are many different parameters that are considered in multiphase modeling including the type of phase coupling and forces acting on dispersed particles. Due to the variety of variables present, the field of multiphase flow modeling is still a continuously developing field with many different approaches in the industry. This type of flow is present everywhere in nature in the air, river flows and in the industry in oil and gas, food production and wastewater treatment. The latter is the topic of focus of this thesis. One device that is used to perform wastewater treatment is the centrifuge decanter separator.

One of the tools used to analyze multiphase flow is computational fluid dynamics (CFD). Recently, the advancements in computer systems as well as the evolution of the field of multiphase flow modeling has made CFD more prominent for simulations involving the centrifuge decanter. Problem solving and concept evaluation are all goals that can be achieved through the effective use of computer-based simulations. All of that combined with its relatively low cost and ever-increasing level of accuracy as models and computing resources evolve makes it an excellent choice for process analysis in the industry.

Alfa Laval - a Sweden headquartered company - develops, designs, and tests several horizontal centrifuges for a multitude of applications. One of these devices is the decanter centrifuge. In the past, the development and modification of the device focused more on experience, experiments and tests. Recently though, simulation-based methods have been used and thus came the idea of using CFD to understand the flow present within the device and suggest possible improvements and modifications that can enhance the device functions, reduce costs and improve product separation through the use of CFD results.

1.1 Objectives

This thesis work investigates the computational fluid dynamics modelling of a multiphase wastewater treatment centrifuge decanter separator. The aim is to:

- Investigate the separator in a more detailed level.
- Develop a useful simulation strategy for the decanter through the use of CFD for multiphase flow taking into account cost, time and accuracy.
- Perform several simulations and analyze the results.
- Study several operation parameters present in the decanter.
- Make suggestions for future simulations for the decanter.

1.2 Scope

The scope of this thesis includes using CFD as a tool for the analysis of the decanter separator from Alfa Laval. The scope of this work does not include physical compartments that require testing in a lab scale such as the material of construction of the decanter, designs of gearboxes and feed accelerators. Additionally, the scope does not include analysis of dimensions that are difficult to change in the decanter design such as the diameters of the bowl cylinder and the screw conveyor.

1.3 Limitations

This thesis uses a general decanter design from Alfa Laval that can be used for future work. Therefore, detailed experimental data does not exist to validate the results. Additionally, the modeling in this thesis is limited to the CFD solver ANSYS Fluent and thus, only the selection of multiphase models present in the software that were used. Due to the computational time and the limited time frame of 20 weeks for this project, it is not feasible to investigate all the possible models and simulation strategies in this work.

1.4 State of the Art

Recently, simulations have been used for centrifuge device analysis. For instance, Euler-Euler multiphase flow simulations using CFD have been used for investigating a two stage centrifuge [1]. Additionally, for centrifugal separation in the drilling industry, CFD has been used in the past for analysis of screw conveyors [2]. Furthermore, three phase simulations using CFD for a tricanter separator containing water, olive oil and olive pomace have been conducted [3]. Lastly, for petroleum refineries, analysis of three phase oil-water-solids systems have been investigated recently using CFD as a tool [4].

2

Decanter Design

The separator at hand is a decanter centrifuge used to separate water from thickened solids for the sewage wastewater treatment industry. Other applications for the device include the mining industry, polymer industry, ethanol production, animal and vegetable protein industry among many others. Figure 2.1 and Figure 2.2 show the decanter design used in this thesis work. The key concept behind the operation is the feeding of a slurry of liquid and suspended solids by using a stationary cylindrical feed tube into a specific fixed position within the bowl. The slurry exits the feed tube into a region in the conveyor called a feed zone which accelerates the mixture as it exits through its three openings. The movement of the phases within the domain involves the solids traveling along the wall of the bowl while the water travels along the helical path of the blades. The separation involves the liquid leaving at one end of the separator and exits through discharge openings while the solids travel to the other end through a conical section called the beach and the dewatered solids exit through openings. The combination of density differences between phases, settling velocities, gravity and centrifugal forces along with friction coefficient differences between bowl walls and solids makes the separation process possible.

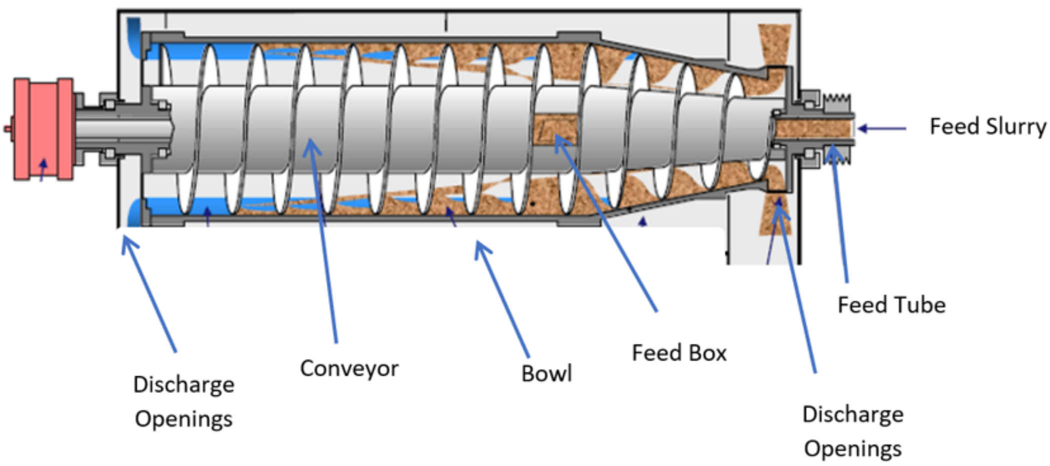

Figure 2.1: Conventional decanter design used for this study. Adopted from [5]. (Courtesy of Alfa-Laval).

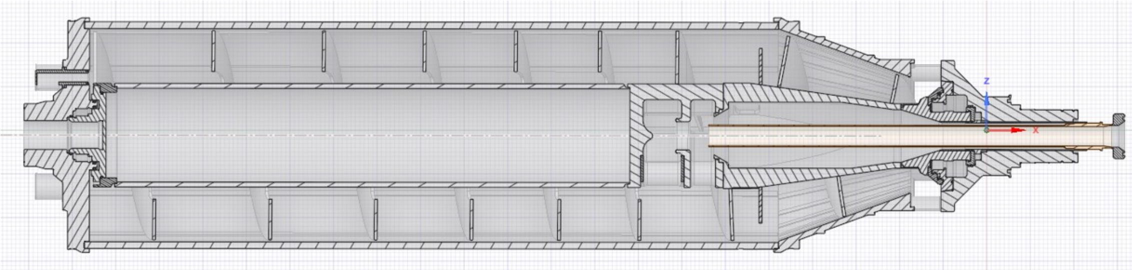

Figure 2.2: CAD model from SpaceClaim direct modeler (SCDM) of the decanter.

There are many parts involved in the design of the centrifuge decanter. For this thesis work, the key parts to be focused on will be summarized below.

2.1 Geometry Description: Bowl

The bowl is a rotating cylindrical compartment that houses the components of the decanter. The cylindrical tube is bolted at each end to discharge ports for the solids and liquids respectively. There are eight discharge ports for the solids while there are five discharge ports for the liquid for this specific decanter arrangement [6].

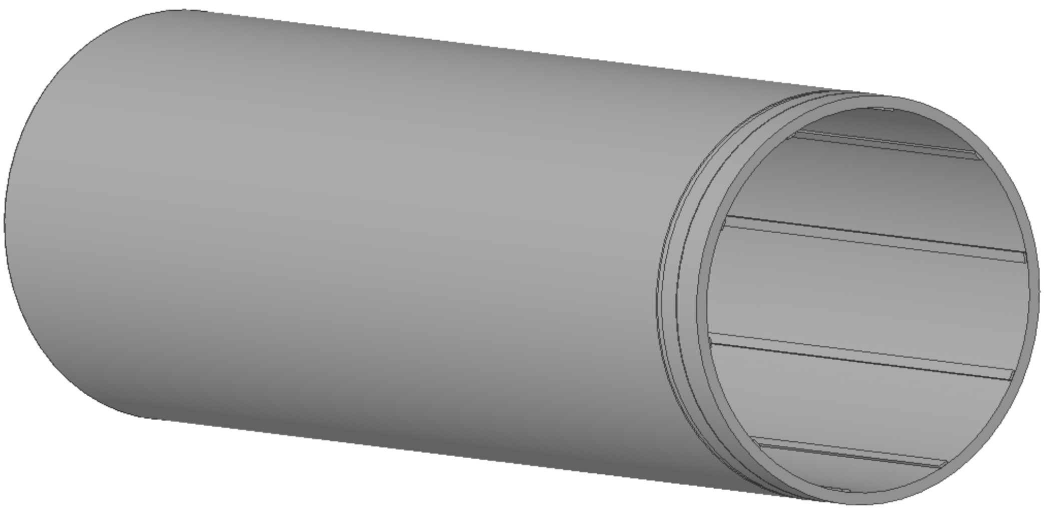

Figure 2.3: CAD model from SpaceClaim direct modeler (SCDM) of the bowl.

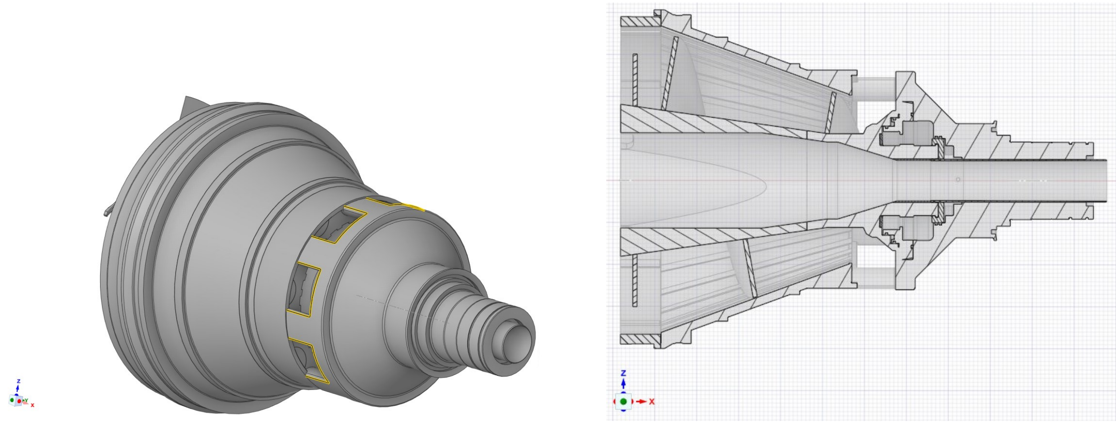

(a) Externals **(b)** Internals

Figure 2.4: CAD model from SpaceClaim direct modeler (SCDM) of the conical section showing the solids' discharge ports.

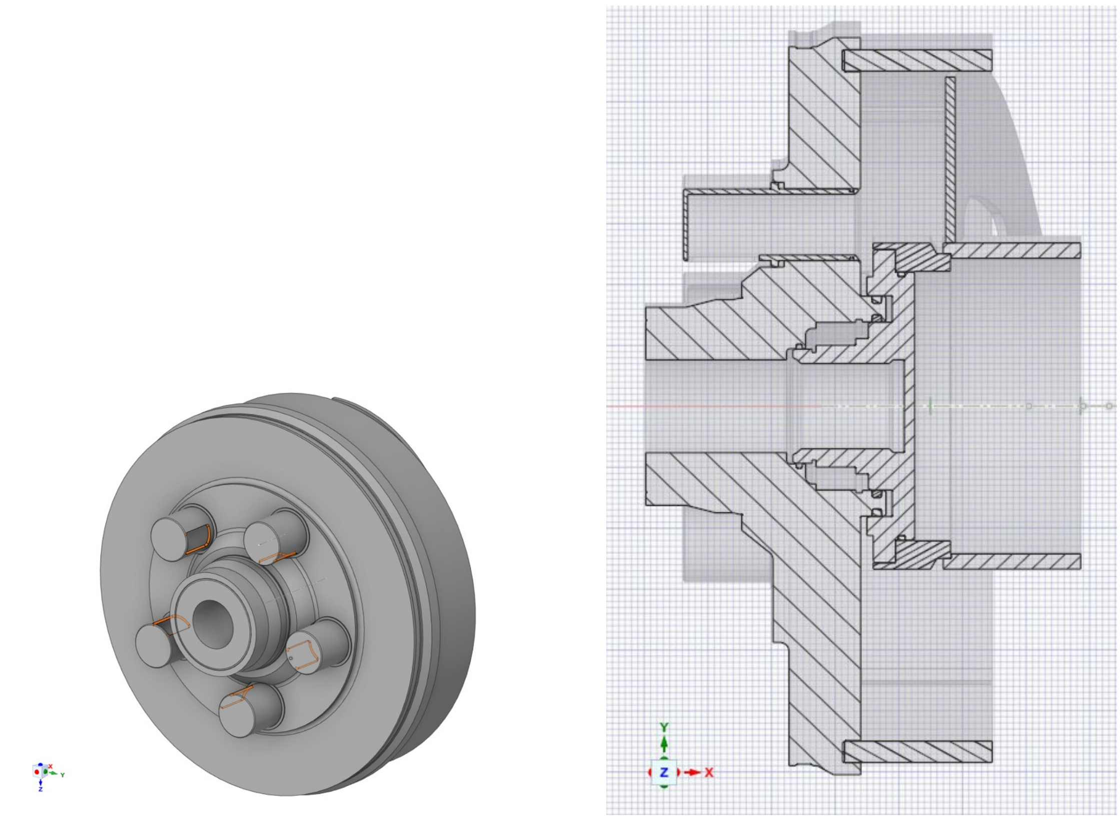

(a) Externals **(b)** Internals

Figure 2.5: CAD models from SpaceClaim direct modeler (SCDM) of the liquid discharge ports.

2.2 Geometry Description: Screw Conveyor

The screw conveyor (or scroll) is in the form of a rotating screw that is fitted inside of the bowl housing with small clearances in-between the bowl's inside wall and the edges of the blades. The conveyor transports the solids along the cylindrical walls of the bowl and accelerates the incoming feed to a speed close to that of the rotating bowl [6].

The screw conveyor is composed of a feed zone that serves as a housing to the incoming mixture that travels transitionally through the feed tube and acts as the first rotational accelerator for the mixture. A protection element called a liner is present in each of the three outlets of the feed zone. It is a high wear and tear region that requires highly resistant materials of construction and is often replaced from time to time. There are three openings of discharge from the feed zone into the conveyor hub with each opening having its own liner that helps in the discharge of the feed [6].

A blade section is arranged in a helical formulation and is attached to the main part of the screw conveyor across the length of the device. The blades are normally perpendicular to the bowl wall and transfer the liquid towards the center of the domain through traveling along the helical path. The incoming mixture accelerates with the existing liquids within the domain until the average velocity is high enough after traveling through the length of the helical path and thus increasing the separation. There are openings in-between the blades and the conveyor hub in this design to control the distance a liquid must travel [7].

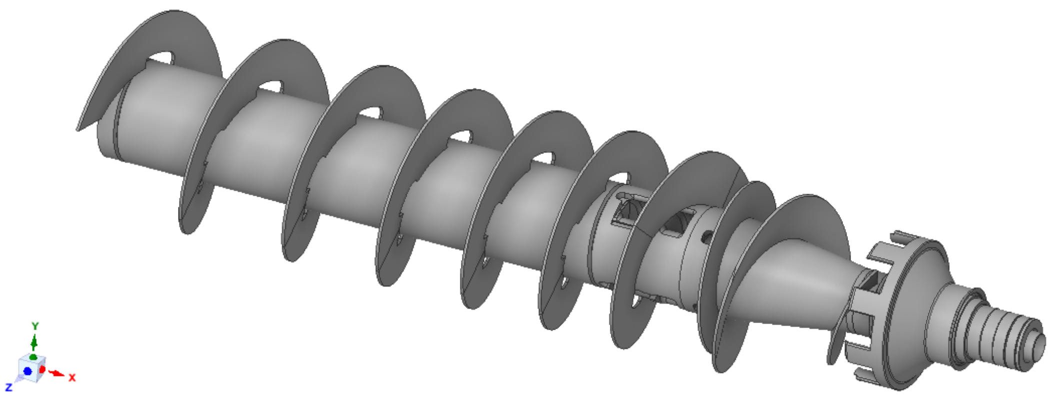

Figure 2.6: CAD model from SpaceClaim direct modeler (SCDM) of the conveyor.

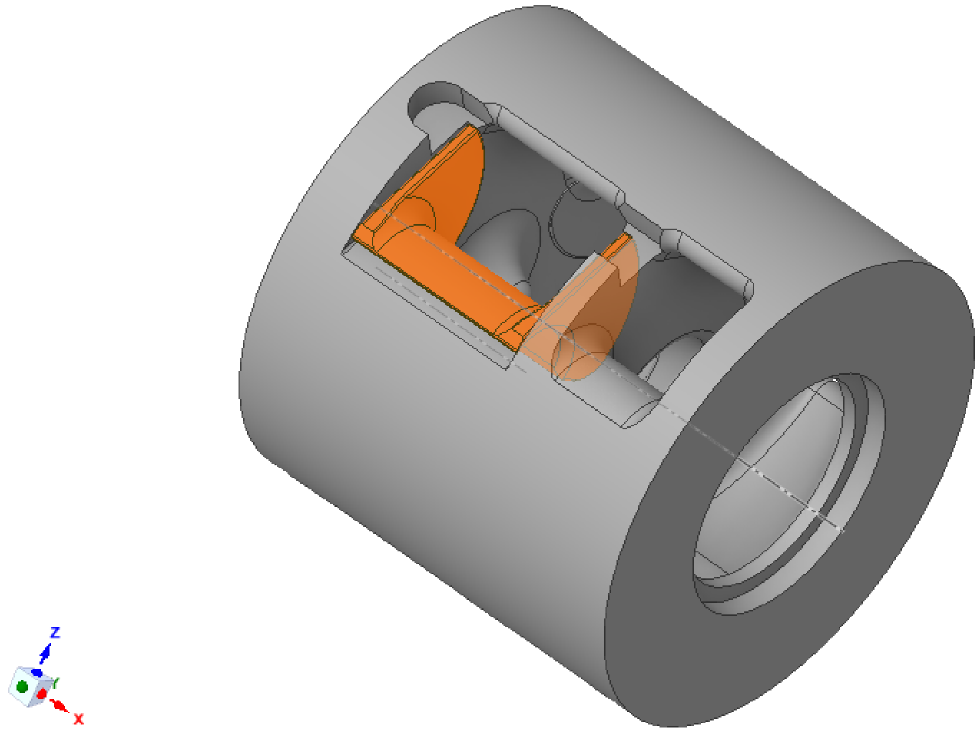

Figure 2.7: CAD model from SpaceClaim direct modeler (SCDM) of a liner location within the feed zone.

3

Theory

In this chapter, the theory involved in CFD and multiphase flow modeling will be discussed alongside the key governing equations used for the decanter separation process and design as well as key information regarding the software in this project.

3.1 Computational Fluid Dynamics (CFD)

Computational fluid dynamics is considered a branch of fluid mechanic studies that uses a combination of data structuring and numerical analysis to both solve and analyze problems that involve fluid flows.

3.1.1 Flow Equations

The governing equations are general and are used for any type of flow simulations. The continuity equation and the Navier-Stokes momentum equations respectively are given in simplified tensor notation form in equation (3.1) and (3.2) [8]. The continuity equation describes the mass conservation within the domain while the Navier-Stokes equations describe the linear momentum conservation.

$$\frac{\partial \rho}{\partial t} + \frac{\partial \rho U_j}{\partial x_j} = 0 \tag{3.1}$$

$$\frac{\partial U_i}{\partial t} + U_i \frac{\partial U_i}{\partial x_j} = -\frac{1}{\rho}\left(\frac{\partial P}{\partial x_i}\right) + \frac{1}{\rho}\left(\frac{\partial \tau_{ji}}{\partial x_j}\right) + g_i \tag{3.2}$$

Additionally, the total energy is balanced by using equation (3.3):

$$\frac{\partial h}{\partial t} = -\frac{\partial}{\partial x_j}\left[hU_j + \lambda \frac{\partial T}{\partial x_j} + \sum_n m_n h_n j_n - \tau_k j U_k\right] + S_h \tag{3.3}$$

3.1.2 Meshing

CFD divides the domain into smaller computational cells that can be in many types including Tetrahedral, Polyhedral, Hexacored and Polyhexacored cells [10]. Figure 3.1 shows Tetrahedral and Hexacored elements. In this project, Polyhexacored cells are used for meshing. This type of mesh is used to connect high quality hexahedrons in the region of the bulk flow to isotropic prisms present in the boundary layers and connects the two regions with traditional polyhedral cells. This significantly reduces the number of elements needed and thus, speeds up the simulations while also maintaining high mesh quality [12].

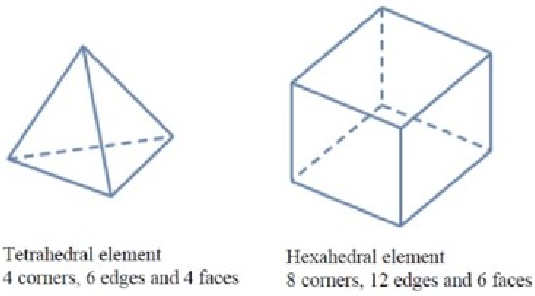

Figure 3.1: Tetrahedral and Hexacored elements. Adapted from [9].

3.1.3 Numerical Aspects

Several different discretization schemes are present in CFD which include [8]:

- **First Order Discretization Scheme:** A good choice for convection dominated flows and good for starting off simulations.

- **Second Order Discretization Scheme:** More accurate than first order but at times can be unstable.

- **QUICK Discretization Scheme:** Higher accuracy than second order but is often limited in terms of compatible mesh types.

The governing equations have strong coupling between the pressure and velocity. Many type of solvers exist and one type is the segregated solver such as SIMPLE (Semi Implicit Method for Pressure Linked Equations). This type uses a purposefully incorrect guess for the pressure to start with and then uses a number of correction factors [8]. An iterative process is used until both momentum and continuity equations match the velocity field. As a result, the simulations using SIMPLE are often slower [10]. Another type of solver is the coupled type in which both momentum and continuity equations are solved in parallel. The total number of iterations for this type of solver is usually less but often needs a larger memory. A choice of a specific scheme is difficult but it can result in a faster simulation [10].

3.1.4 Turbulent Flow

Many of the flows found in nature and the industry involve turbulent flows in which random variations of time scales and space scales are encountered [8]. Due to the complex nature of turbulent flows involved within CFD, modeling is often required to obtain a solution. Direct Numerical Simulations (DNS) involves solving the unsteady Navier-Stokes equations thus, it is very computationally costly and unpractical for engineering purposes. Large eddy simulations (LES) use the idea of filtering-out the smallest of turbulent time and length scales thus, solving only for the larger ones. However, LES is limited with requirements of very fine grids and judging the quality of results is often challenging and ambiguous. Modeling using Reynolds Averaged Navier-Stokes models is thus the most common method present in the industry. The idea is to model modified Navier-Stokes equations that have resulted from the removal of small scale fluctuations present in the turbulent flow. The modeling is often achieved by using empirical closures to account for the modified terms in the governing equations.

One important dimensionless number used in the analysis of turbulence is the Reynolds number:

$$Re = \frac{\rho L V}{\mu} \tag{3.4}$$

A value higher than 2000 for the Reynolds number for pipe flow presents turbulent flow while less than that presents laminar flow.

For the inlet of the decanter in this project, the Reynolds number is estimated to be around 200000 which shows turbulence in that region. This is an indication of the importance of the choice of turbulence boundary conditions as the slurry is introduced into the domain.

Two equation models are the most common and well-known turbulence models which include the k-ϵ, k-ω, Realizible k-ϵ, RNG k-ϵ. Additionally, a six equation model named the Reynolds Stress Model is common as well. The simulations used for this project included the use of the k-ω model. This model uses the specific dissipation (ω) and is given by [8]:

$$\omega \approx \frac{\epsilon}{k} \tag{3.5}$$

Which represents the inverse of the dissipation time scale.

The two equations modeled in this model are the k-equation and ω-equation given respectively in equation (3.6) and (3.7) [8]:

$$\frac{\partial k}{\partial t} + \langle U_j \rangle \frac{\partial k}{\partial x_j} = \upsilon_T \left[\left(\frac{\partial \langle U_i \rangle}{\partial x_j} + \frac{\partial \langle U_j \rangle}{\partial x_i} \right) \frac{\partial \langle U_i \rangle}{\partial x_j} \right] - \beta k \omega + \frac{\partial}{\partial x_j} \left[\left(\upsilon + \frac{\upsilon_T}{\sigma_k} \right) \frac{\partial k}{\partial x_j} \right] \tag{3.6}$$

$$\frac{\partial \omega}{\partial t} + \langle U_j \rangle \frac{\partial \omega}{\partial x_j} = \alpha \frac{\omega}{k} \upsilon_T \left[\left(\frac{\partial \langle U_i \rangle}{\partial x_j} + \frac{\partial \langle U_j \rangle}{\partial x_i} \right) \frac{\partial \langle U_i \rangle}{\partial x_j} \right] - \beta^* \omega^2 + \frac{\partial}{\partial x_j} \left[\left(\upsilon + \frac{\upsilon_T}{\sigma_\omega} \right) \frac{\partial \omega}{\partial x_j} \right] \tag{3.7}$$

The advantages the k-ω model has include not needing wall functions or special low Re number modifications when in the viscous sub layer which happens in regions with relatively low turbulence [8]. A limitation it has is the fact that a very fine mesh must be used near the wall with a first grid less than a value of y^+=5.

The shear stress transport (SST) variant of the k-ω model accounts for the transport of the wall shear stress by adding it to the turbulent viscosity expression by modification in the form of [10]:

$$\mu_t = \frac{\rho k}{\omega} \frac{1}{max[\frac{1}{\alpha} \frac{SF_2}{\alpha_1 \omega}]} \tag{3.8}$$

The k-ω model is modified as follows using SST [11] :

$$\frac{\partial k}{\partial t} + U_j \frac{\partial k}{\partial x_j} = P_k - \beta^* k\omega + \frac{\partial}{\partial x_j}\left[\left(\upsilon + \sigma_k \upsilon_T\right)\frac{\partial k}{\partial x_j}\right] + S_k \tag{3.9}$$

$$\frac{\partial \omega}{\partial t} + U_j \frac{\partial \omega}{\partial x_j} = \alpha S^2 - \beta\omega^2 + \frac{\partial}{\partial x_j}\left[\left(\upsilon + \sigma_\omega \upsilon_T\right)\frac{\partial \omega}{\partial x_j}\right] + 2\left(1 - F_1\right)\sigma_\omega^2 \frac{1}{\omega}\frac{\partial k}{\partial x_j}\frac{\partial \omega}{\partial x_j} + S_\omega \tag{3.10}$$

Where S_k and S_ω are additional source terms for turbulence and specific dissipation respectively arising from particle movement. Different source terms are present depending on the choice of multiphase models.

3.1.5 Near-Wall Modeling

To solve the near wall region where some turbulence models such as the k-ϵ model fail, there are two approaches which are either modeling a first grid point near but not at the wall using different types of boundary conditions in the form of wall functions. The other approach involves modifying the turbulence model equations to solve the viscous near wall regions.

At the wall, the production of turbulent kinetic energy is zero while the rate of dissipation is at its peak and it decreases as we move closer to the bulk flow [8]. The best way to express physical properties near the wall is to divide the region into smaller sub-layers and use individual characteristic scales for the velocity and length scales.

y^+ is often the measure of the distance from the wall where a value of zero is at the wall. It represents a physical extent for each sub-layer and is a determination of the viscous-effected domain near the wall.

The boundary layer near the wall involves three sub-layer regions:

- **Viscous sub-layer:** the inner most layer closest to the wall that is laminar where molecular viscosity plays a role and all the stress is due to viscous shear. The y^+ ranges from $0<y^+<5$. In this layer, the dissipation rate is much larger than the production of turbulent kinetic energy.

- **Buffer sub-layer:** the transition region from the laminar near wall behaviour to the turbulent behaviour in the bulk flow. The y^+ ranges from $5<y^+<30$. the production of turbulent kinetic energy reaches its peak somewhere within this layer.

- **Fully turbulent sub-layer:** the outer most layer furthest from the wall where viscous effects are negligible and turbulence plays the biggest role. The y^+ ranges from $y^+>30$. In this layer, the production of turbulent kinetic energy and dissipation rates are almost equal.

3.2 Multiphase Flow Modeling

Multiphase flow modeling is characterized by the presence of two or more phases that interact in different ways. There are several characterizations, forces acting within the system, types of phase interaction and coupling as well as particle interactions within a domain. All these components will in turn lead to a choice of modeling approach in CFD. This section focuses on the key theory involved with these elements.

3.2.1 Key Characteristics

For multiphase flow, there are several characteristics that are discussed which help in the choice of multiphase flow models. Key characteristics are discussed below.

3.2.1.1 Flow Regime Types

Multiphase flow regimes are divided into two key types as seen in Figure 3.2. The first is separated flow in which phases are separated with only very few interfaces present. The second is dispersed flow in which one phase is in the form of particles or droplets with many interfaces present. Dispersed flow is generally either dilute with large spacing between particles or dense with smaller spacing and particle-particle interactions becoming important.

Figure 3.2: Flow regimes for multiphase flow. Adapted from [13].

3.2.1.2 Volume Fraction

The volume fraction is a ratio between the volume of one of the phases to that of the total mixture [8]:

$$\alpha_d = \frac{V_d}{V_{tot}} \tag{3.11}$$

3.2.1.3 Stokes Number

The Stokes number is a dimensionless number used to express the ratio in terms of time scales between the dispersed and continuous phases. It determines how independently the two phases act relative to one another which in turn helps in choosing a suitable multiphase model. One type of Stokes number is the turbulent Stokes number defined as the ratio between dispersed and turbulence time scales and is given by [8]:

$$St_T = \frac{\tau_d}{\tau_T} \tag{3.12}$$

The time scales of the dispersed phase and turbulence respectively are written as:

$$\tau_d = \frac{\rho_d D^2}{18\mu_f} \tag{3.13}$$

$$\tau_T = \frac{k}{\epsilon} \tag{3.14}$$

Additionally, the flow Stokes number is often used [10]:

$$St = \frac{\tau_d}{t_s} \tag{3.15}$$

Where t_s is the system's response time given as:

$$t_s = \frac{L_s}{V_s} \tag{3.16}$$

Estimations from equations (3.12), (3.15) and (3.16) resulted in a flow Stokes number of 0.239. A Stokes number value less than 1 indicates that particles tend to follow the continuous phase more closely and thus, using the mixture model is applicable for the decanter presented in this project [10]. However, practical considerations such as computational time became more influential in choosing the less computationally expensive mixture model.

3.2.1.4 Additional Characteristics of Multiphase Flow

Other key characteristics involve the size and shape of particles, the distance between particles, mixture densities and the mass loading.

3.2.2 Phase Coupling

Phase coupling can be summarized as the interactions of the dispersed phase within itself and with the continuous phase. Phase coupling in multiphase flow can be categorized into several types. One way coupling occurs when only the effect of the continuous phase on the dispersed particles is important and the effect of particle-particle interactions is negligible. Additionally, two way coupling occurs when the volume fraction of the dispersed phase is large enough to start effecting the average density which results in effects of dispersed particles on the continuous phase. Furthermore, four way coupling happens when the volume fraction of dispersed phase is large enough which in turn forces particle-particle interactions to be accounted for.

3.2.3 Multiphase Models

As mentioned earlier, the modeling involved in multiphase flow is often very complex and uncertain. In many applications, limitations in terms of time and computational power influences the choice of multiphase models. Important models that were used during the course of this thesis are presented below.

3.2.3.1 Euler-Euler Model

The Eulerian model allows for the modeling of phases separately while at the same time accounts for the interactions present. The phases are all treated as continuous phases and are solved with each having its own continuity and momentum equations. It is suitable for complex flows and is considered the most general of the models. However, it is the most computationally costly model and is considerably less stable than others. The only limitation on the number of secondary phases that can be used in this model is the available computational memory and the behavior of convergence. The pressure is shared by all phases and many interphase drag coefficient functions are available [8].

The model has the following governing equations:

$$\sum_k \alpha_k = 1 \tag{3.17}$$

$$\frac{\partial \alpha_k \rho_k}{\partial_t} + \frac{\partial \alpha_k \rho_k U_{i,k}}{\partial x_i} = -\sum_{l=1}^{p} m_{kl} - m_{lk} \tag{3.18}$$

$$\frac{\partial \alpha_k \rho_k U_{i,k}}{\partial_t} + \frac{\partial \alpha_k \rho_k U_{i,k} U_{j,k}}{\partial x_j} = -\alpha_k \frac{\partial P}{\partial x_i} + \frac{\partial \alpha_k \tau_{ij,k}}{\partial x_k} + \alpha_k \rho_k g_i + \sum_l^N \Big(K_{lk}(U_{i,k} - U_{i,l}) \Big) + F_{i,k} \tag{3.19}$$

The transfer of momentum for eulerian particle collisions is modeled by a specific coefficient that is a complex function of many different parameters and is given by the expression:

$$K_{lk} = \frac{3(1+e_{lk})(\frac{\pi}{2} + C_{fr,lk}\frac{\pi^2}{8})\alpha_k \rho_k \alpha_l \rho_l (D_k + D_l)^2 g_{0,lk}}{2\pi(\rho_l D_l^3 + \rho_k D_k^3)} |U_f - U_d| \tag{3.20}$$

The collisions between particles determines the quality of viscosity modeling within a multiphase system. There are three main mechanisms for the transfer of viscosity which are movement through granular kinetic effects, collisions between particles and friction between particles. Expressions for the three mechanism are given in equations (3.21), (3.22) and (3.23) respectively [8]. Additionally, granular temperature and particle rheology can influence the elasticity of particle collisions.

$$\mu_{d,kin} = \frac{\alpha_d d_d \rho_d \sqrt{\theta \pi}}{6(3-e_d)} \Big[1 + \frac{2}{5}(1+e_d)(3e_d - 1)\alpha_d g_0 \Big] \tag{3.21}$$

$$\mu_{d,col} = \frac{4}{5} \alpha_d \rho_d d_d g_0 (1+e_d)(\frac{\theta}{\pi})^{\frac{1}{2}} \tag{3.22}$$

$$\mu_{d,fr} = \frac{p_d sin\phi}{2\sqrt{I_{2D}}} \tag{3.23}$$

The total viscosity for the dispersed phase is thus given by:

$$\mu_d = \mu_{d,kin} + \mu_{d,col} + \mu_{d,fr} \tag{3.24}$$

Furthermore, the volume fraction of the dispersed phase influences the radial distribution in the expression [8]:

$$g_0 = \Big[1 - (\frac{\alpha_d}{\alpha_{d,max}})^{\frac{1}{3}} \Big]^{-1} \tag{3.25}$$

3.2.3.2 Mixture Model

The mixture model is considered a simplified type of the Euler-Euler model. The mixture model uses mixture based properties to solve the transport equations. The phases can be modeled to move with different slip and drift velocities. It often needs a strong interaction between phases and assumes very strong coupling. It can be used as a good initial condition for the Euler-Euler model since it is more stable and faster to simulate. The governing equations solved by the mixture model involve [8]:

$$\frac{\partial \rho_m}{\partial t} + \frac{\partial \rho_m U_{i,m}}{\partial x_i} = 0 \tag{3.26}$$

$$\frac{\partial \rho_m U_{i,m}}{\partial t} + \frac{\rho \partial_m U_{i,m} U_{j,m}}{\partial x_j} = -\frac{\partial P}{\partial x_i} + \frac{\tau_{ij,m}}{\partial x_j} + \rho_m g_i - \frac{\partial \sum_k \alpha_k \rho_k U_{i,dr,k} U_{j,dr,k}}{\partial x_j} \tag{3.27}$$

The mixture properties are typically averaged by volume fraction:

$$\mu_m = \sum_m \alpha_k \mu_k \tag{3.28}$$

3.3 Decanter Separator

The decanter centrifuge has several design and operating parameters. Key ones are discussed in this section.

3.3.1 Rotation and Differential Speed

One of the concepts that create separation between the two phases is the differences in rotational speed between the bowl wall and the conveyor. The bowl speed defines the centrifugal acceleration in the cylindrical bowl geometry by the following relation [7]:

$$a = \omega^2 r_o \tag{3.29}$$

In terms of differential rotational speeds, very low differential speeds between the bowl and conveyor is usually resulting in thicker layers of settled solids which would result in a decrease in water and solid recovery efficiency. On the other hand, a too large differential speed can lead to re-suspended solids in the domain. Therefore, an optimal range for the differential speed should be set depending on the process requirements in the form of the solid's clarity. Often in the decanter there is a fitted variable speed drive that allows for easier adjustments in the optimization process. The relation between the differential and axial transportation speeds is given as [7]:

$$v = \frac{G\Delta}{2\pi} \tag{3.30}$$

Where v is the axial transport velocity, G is the distance between two consecutive blade edges and Δ is the rotational speed difference between the bowl and the conveyor/blade assembly.

3.3.2 Geometrical Dimensions

Since the settling of solids happens in the cylindrical section of the bowl, the inner surface area of that section is to be considered by [7]:

$$A_{Cyl} = 2\pi r_o L_{Cyl} \tag{3.31}$$

Additionally, the distance in-between blade sections in the conveyor scroll is also a key parameter to be considered. The distance influences the axial speed and the thickness of solids' discharge as discussed. One parameter to be looked at is the pitch angle which effects the circumferential force applied to the solids. The pitch angle can be expressed by [7]:

$$\alpha = \tan^{-1}\left(\frac{G}{2\pi r_o}\right) \tag{3.32}$$

This angle is different in conventional decanters in the conical beach section compared to the cylindrical part. This is done to adjust the residence time in the conical part and improve separation.

3.3.3 Stokes' law

Several parameters determine the settling speed of a particle inside a vessel. These parameters are the the diameter of particles, densities and viscosities of the liquid and solid components and the applied gravitational force. The Stokes law is used to give an expression for the settling velocity of suspended spherically-shaped particles:

$$V_g = \frac{d^2(\rho_p - \rho_l)}{18\mu} g \tag{3.33}$$

The settling velocity is often a key parameter in understanding the overall separation efficiency in the decanter and it can be seen from equation (3.33) that the diameter of the particles has the larger effect due to it being raised to power of two. The idea would be to increase the size of particles and thus, reduce the total settling time of solid particles. Additionally, the viscosity of the liquid can be adjusted through changes in temperature which also adjusts the settling velocities and therefore affects the separation efficiency.

3.4 Software

In this section, the software used in this thesis are described. For geometry, ANSYS SpaceClaim was used while mesh generation was done using ANSYS Fluent Meshing. The CFD commercial solver ANSYS Fluent was used for the simulations.

3.4.1 SpaceClaim Direct Modeler (SCDM)

ANSYS SpaceClaim is a 3D modeling software used for the creation, modification and for importing different types of geometries and is a leader for rapid concept designing and 3D geometry modifications. The direct nature of the software as well as its modern nature and friendly user interface are considered its key features. The interface has four main tools that are the essential components for most applications which are the pull, move, fill and combine tools [14].

3.4.2 Fluent Meshing

ANSYS Fluent Meshing is a robust, modern unstructured grid generation software. Fluent Meshing is a powerful tool used to generate meshes of high quality and accuracy for 3D geometries. It has a type of single window simple to use workflow that reduces the burden on the user to come-up with manual parameters for the mesh. The workflow helps in terms of flexibility of mixing and matching different mesh methods as well as being able to fix errors quicker. One workflow type is the watertight workflow which is the most commonly used and allows for minimum clean-up and modifications from the user which speeds up the process [15].

3.4.3 Fluent

ANSYS Fluent is an industry leading CFD solver known for its advanced physics modeling capabilities [10]. Fluent has three types of multiphase models available which are the VOF, Mixture and Eulerian models. Also, a discrete particle tracking model can be used in Fluent. Multiple drag, lift, virtual mass and surface tension coefficients are available to choose from as well as multiple types of population balance options and interfacial area models.

Types of pressure-velocity solvers present include segregated and coupled solvers and types of spatial discretization schemes include first, second and third order MUSCL. Pseudo transient is also available as a transient formulation method. Several types of turbulence models can be used which include the k-ω in standard, GEKO, BSL or SST formulations. Additionally, the standard k-ϵ, RNG k-ϵ, realizable k-ϵ or the Reynolds stress model can be used.

Fluent offers several types of boundary conditions such as velocity inlet, pressure outlet, outflow and symmetry. In addition, turbulent boundary conditions such as intensity and length scale, viscosity ratio or hydraulic diameter.

4
Methodology

In this chapter, the methodology in terms of the geometrical dimensions of the decanter, the mesh used, the boundary conditions, the simulation strategy used in Fluent and the criteria used to judge convergence and simulation evaluation are discussed.

4.1 Geometry

The available geometry needed to be prepared before the generation of meshes. The complex nature of the geometry made it a challenging and time-consuming step in the setup. The process in SpaceClaim included simplification of some regions such as the liner outlet in the conveyor, combining different parts into one body and extracting the targeted fluid zone.
The key dimensions of the decanter include a feed tube diameter (D) , the full length of the geometry along with the diameter of the external bowl wall is as shown in Figure 4.1. Figure 4.2 shows the dimensions associated with the helical blade region.
The first half of the project involved using a smaller portion of the full geometry in order to simplify the first simulations and to test different strategies in the simulations that would later on be used for the full decanter. The sectioned decanter used for the first half of the project is shown in Figure 4.3 and Figure 4.4.

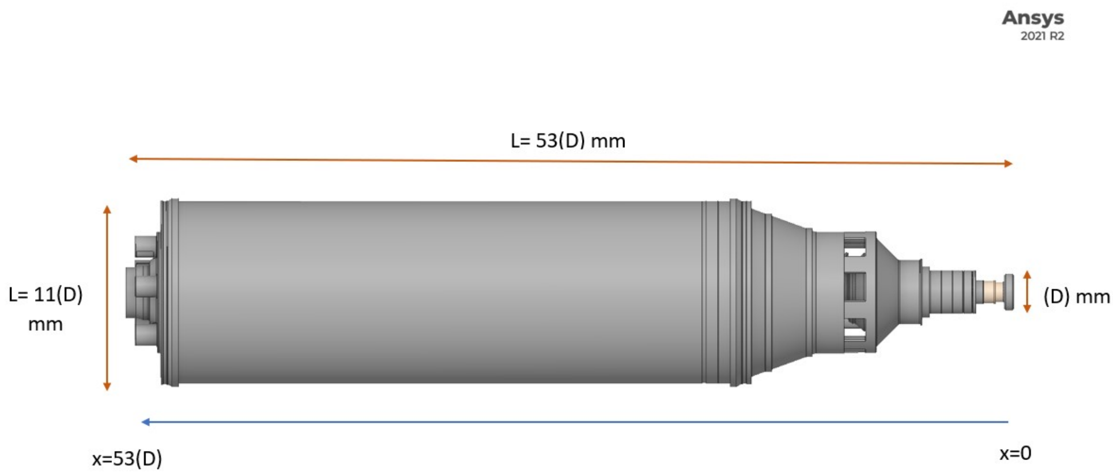

Figure 4.1: Main dimensions of the geometry.

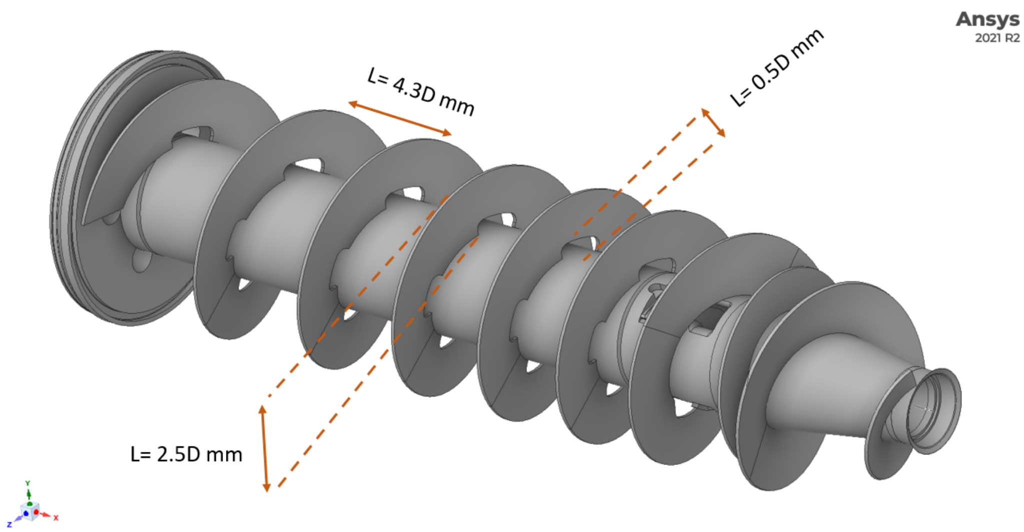

Figure 4.2: Dimensions in the blade section.

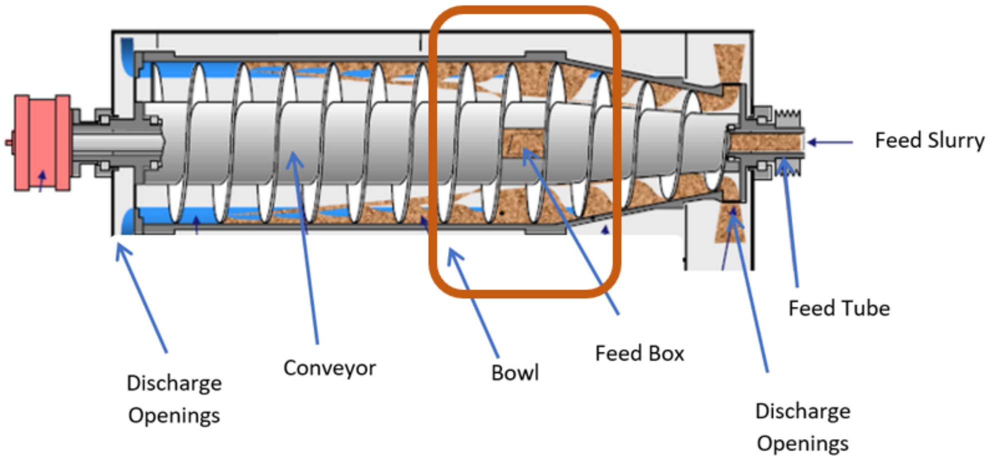

Figure 4.3: Approximate location of the sectioned decanter.

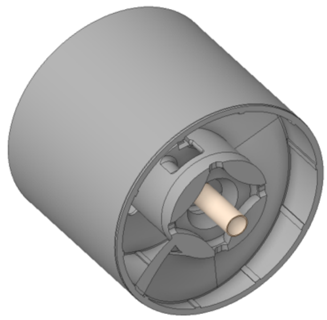

(a) The sectioned decanter geometry.

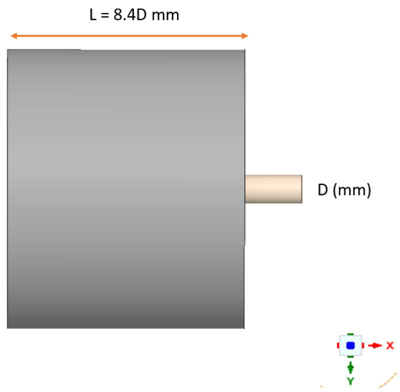

(b) Main dimensions of the sectioned decanter.

Figure 4.4: The sectioned decanter.

4.2 Mesh

The mesh used for the full decanter is composed of poly-hexacored cells which results in a decrease in the total element count compared to conventional hexacored mesh [12]. The statistics for the mesh for both the sectioned and full geometry are presented in Table 4.1. The cell distribution for the surface mesh is shown and several cut plane views of the mesh are presented in Figure 4.5.

Mesh Metric	Sectioned Decanter	Full Decanter
Surface Mesh min. Element Size	0.25 mm	1.81 mm
Surface Mesh max. Element Size	8 mm	29.04 mm
Cells per Gap	3	2
Proximity Type	Cells and Edges	Cells and Edges
Boundary Transition Type	Smooth Transition	Smooth Transition
N.o Boundary Layers	3	5
Growth Rate	1.2	1.2
Min. Cell size	0.25 mm	1.81 mm
Max. Cell size	8 mm	14.50 mm
Min. Orthogonal Quality	0.18	0.14
Max. Skewness	0.77	0.79
N.o Cells	2,488,147 cells	8,363,932 cells

Table 4.1: Mesh statistics for the sectioned and full decanter.

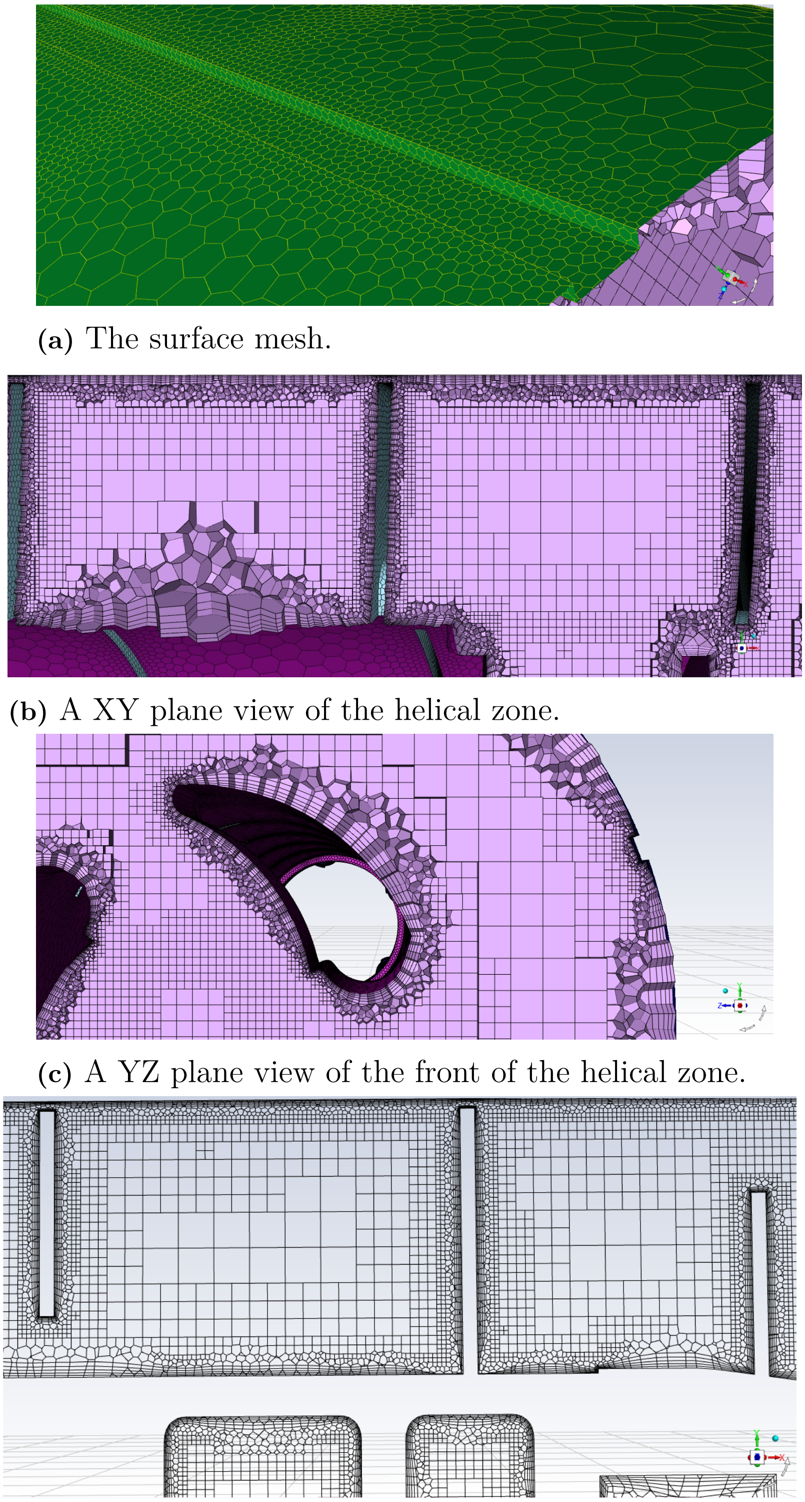

(a) The surface mesh.

(b) A XY plane view of the helical zone.

(c) A YZ plane view of the front of the helical zone.

(d) A XY plane view showing the transition of the poly-hexacored mesh.

Figure 4.5: The used mesh for the full geometry.

4.3 Simulation Strategy

For the first part of the project involving the sectioned geometry, several simulation strategies were tested and systematically altered in Fluent in order to investigate effects and use the most suitable approach later for the full decanter. These strategies for the sectioned geometry part included testing different multiphase models, turbulence models, pressure-velocity formulations and stability of steady state and pseudo-transit solutions.The choice of strategy included recommendations from the literature, ANSYS Fluent and from strategies previously used for similar cases at EDR&Medeso. Transient simulations were not ran in this project due to computational time constraints. The courant number and the time scale factor for the steady state and pesudo-transit simulations respectively were changed accordingly to obtain faster convergence. Table 4.2 shows the simulation strategies used for the sectioned decanter.

For the full decanter, it was found through the tests done for the sectioned part that a coupled pressure-velocity solver, SST k-ω turbulence model and due to stability criteria, a mixture multiphase model were the strategies implemented for the full geometry simulations. Table 4.3 summarizes the simulation strategies used.

Simulation Run	Strategy
1.	Pesudo Transit - Single phase - No rotation - SIMPLE Velocity and Pressure SST k-ω turblence model - Second order dicretization Scheme
2.	Added rotation to the walls
3.	Switched to multiphase mixture model - No rotation
4.	Changed to coupled velocity and pressure formulation PRESTO! pressure spital dicretization
5.	Added small amount of rotation
6.	Switched to multiphase Euler-Euler model - No rotation
7.	Generated a new mesh to improve convergence
8.	Turned off volume fraction equations to start simulation
9.	Once stable, turned volume fraction equations on

Table 4.2: Simulation strategy for the sectioned decanter.

Simulation Run	Strategy
1.	Pesudo Transit - Single phase - No rotation - Coupled Velocity and Pressure SST k-ω turbulence model - First order dicretization Scheme
2.	Added rotation in increments up to full speed
3.	Switched to steady state coupled solution
4.	Switched outlet boundary condition to mass outlet
5.	Switched outlet boundary condition to outflow
6.	Switched Outlet Boundary Condition back to pressure outlet with targeted mass flow values for outlets
7.	Started a new solution with slower steps in rotation ramping
8.	Switched to multiphase mixture for full rotation with outlet boundary condition pressure values from each step of the rotation in the single phase case

Table 4.3: Simulation strategy for the full decanter.

4.4 Boundary Conditions

The boundary conditions used for the simulations involved using a velocity inlet boundary condition with a specified volume fraction for the solids. Furthermore, the turbulence boundary condition of intensity and hydraulic diameter were used for the inlet. The no-slip condition was used for the shear condition for the walls in the domain. Additionally, for the outlet boundary conditions, three different types were tested at different points of the project:

- **Pressure Outlet:** The gauge pressure was set at 0 Pa for both outlets and the target mass flow option was often used. In multiphase flow simulations, the pressure outlet values from the single-phase case were used as a boundary condition to replicate the flow.

- **Outlet Mass Flow:** For few simulations, the mass flow boundary condition was tested in order to direct the majority of water into the desired outlet. Though, the simulations have resulted in extremely large flow rates in the water side outlet.

- **Outlet Outflow:** For few simulation, the outflow boundary condition was used as an alternative to the mass flow outlet condition. However, simulations resulted in extremely high pressures in the water side outlet.

The rotation in the domain was set through changing the wall motion boundary condition for the blades/conveyor assembly, the bowl and the stationary inlet tube. This was done through imposing with the moving reference frame (MRF) method. All walls were set to rotate with the positive X-axis as the rotation axis of the domain. Figure 4.6 shows the rotational directions used. The strategy to implement the rotation was as follows:

- **Blades/Conveyor Assembly:** Set as a moving wall with an absolute motion rotation in the anti-clockwise direction.

- **The Bowl:** Set as a moving wall with with a rotation that is relative to the adjacent cell zone in the clockwise direction.

- **The Stationary Inlet Tube:** Set as an absolute moving wall with zero rotation speed to keep it stationary.

In addition, the fluid cell-zone in the domain was set with a frame motion with a rotational axis direction as the positive X-axis and an absolute relative specification to the cell zone. The diameter of the solid particles is 0.001 m. Table 4.4 summarizes implemented the boundary condition values while Table 4.5 shows the properties for the mixture slurry analyzed in this project.

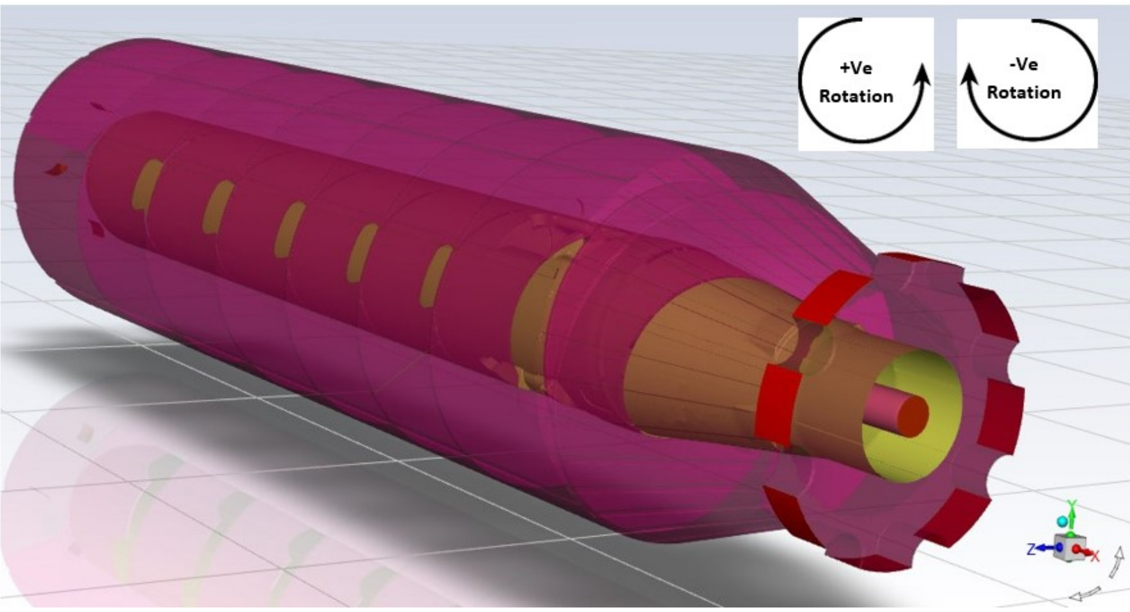

Figure 4.6: The direction of rotation used with the indicated signs.

Boundary Condition	Value
Velocity Inlet	4.78 m/s
Volume Fraction of Solids	2.5 %
Blades/Conveyor	Max. rotation of 3785 rpm
Bowl	Max. rotation of -3800 rpm
Fluid Cell Zone	Max. rotation of -3800 rpm

Table 4.4: Boundary conditions.

Property	Value
Water Density	1000.35 kg/m^3
Water Viscosity	1.005e$^{-3}Pa.s$
Solids Density	1450 kg/m^3
Solids Viscosity	2.001e$^{-2}Pa.s$

Table 4.5: Mixture slurry properties.

4.5 Convergence and Evaluation

Convergence was monitored through the residuals of the momentum, continuity, turbulence and volume fraction equations. However, the convergence criteria of 10^-5 was rarely reached during simulations due to the complex nature and in instances, stable residuals were reached but the validity of results needed to be checked. Therefore, other methods were used to judge the convergence through using report plot monitors including that of outlet pressures, outlet mass flows and wall shear stresses with the aim of reaching a stable solution.

Simulations were evaluated based on three different simulation criteria which were the computational time, accuracy of solution and stability. The time requirement can be judged based on how long a stable or converged solution was reached while the accuracy criterion was evaluated through checking different parameters fields. Examples included the assessment of velocity and pressure magnitudes as well as material balance and direction of flow through using amounts of solids and water coming out in each outlet side of the decanter or through the use of X-direction velocity fields. The stability criterion was judged based on how difficult it was to obtain a converged solution. For instance, an Euler-Euler multiphase model simulation was much more difficult to stabilise and thus a mixture model simulation was judged as better in terms of simulation stability.

5
Results

In this Chapter, the results of the simulations are presented and analyzed. In Section 5.1, the results for the simulations done for the sectioned decanter are discussed while in Section 5.2, the results of the full decanter simulations are presented.

5.1 Sectioned Decanter

This first half of this project involved using a sectioned part of the decanter as mentioned before. Many simulations were conducted in order to evalute different mesh and simulations strategies. In this section, the key simulations will be showed. Figure 5.1 shows the location of the both outlet sides as well as the naming that will be used for the upcoming analysis of the sectioned geometry.

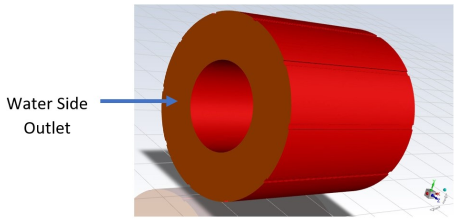

(a) Location of water side outlet.

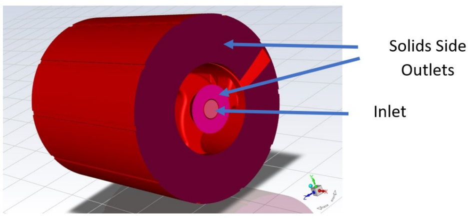

(b) Location of solids' side outlet.

Figure 5.1: Location and naming of outlets for the sectioned decanter.

5.1.1 Multiphase Case

The multiphase test simulations were conducted with both the mixture model and the Euler-Euler model. Second order upwind scheme was used with no rotation applied to the walls. Later on, rotation with 2.5% of the full speed was applied in order to test the flow field. In this subsection, results between the two multiphase models will be compared and the effect of adding rotation will be analyzed.

5.1.1.1 Flow Field

The velocity field for the solids of both the mixture and Euler-Euler models are compared in Figure 5.2 for a cross section for a non rotating case. It can be seen that there is a slight difference in the maximum velocity with the Euler-Euler model having a maximum velocity of 7.49 m/s while the mixture model has a maximum velocity of 7.01 m/s. The field shows similar trends for both models with the flow hitting the wall of the feed zone as it exits the feed tube with re-circulation happening. The stability of the model along with the computational time became a major factor later on for choosing the mixture model instead of the Euler-Euler model. Furthermore, if detailed experimental data were to be used to validate the solution, it is possible that the Euler-Euler would provide more accuracy.

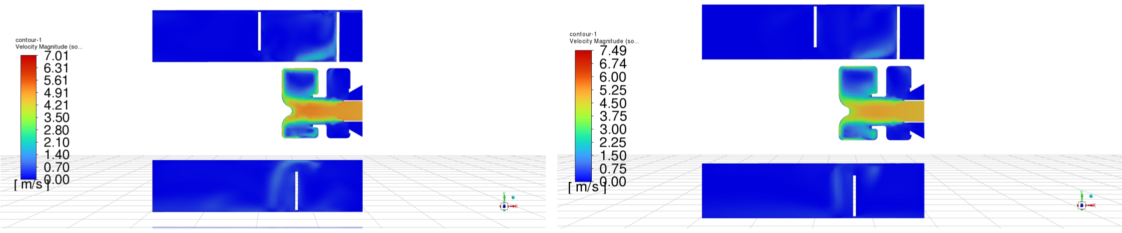

(a) Mixture model.

(b) Euler-Euler model.

Figure 5.2: Solids' velocity distribution field.

5.1.1.2 Effect of Rotation

Figure 5.3 shows the blade section view for the velocity for a non rotating mixture model case compared to a rotation of 2.5% of the full rotation for the bowl and conveyor/blades assembly. The results show that the centrifugal forces added through the rotation make it so the maximum velocities are distributed along the wall of the rotating bowl as expected by the phenomena. The solids account for the majority of the flow along the bowl wall and even with a extremely small rotation this showed that the phenomena is expected to be replicated with the full geometry and with higher rotational speeds.

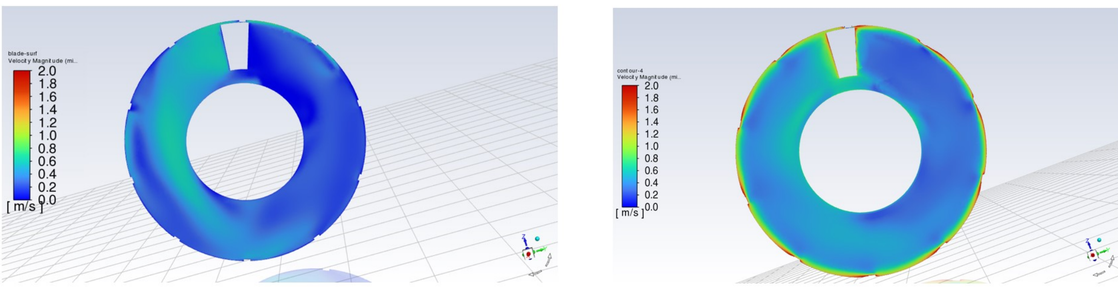

(a) No Rotation.

(b) 2.5% of Full Rotation.

Figure 5.3: Analysis of rotation along a blade section.

Figure 5.4 shows the volume fraction distribution of the solids for the low rotation case compared to a no rotation case using the mixture model. As seen, with the rotation there is a more even distribution for the solids volume fraction to where the largest volume fractions are present along the scroll in the bowl wall which replicates the reality well. This combined with there being more of the solids towards the positive X-axis outlet side shows the separation phenomena for the solids is replicated to an extent with this simulation. It is important to note that ANSYS Fluent extrapolates values to the first cell point in the mesh when a wall is used for displaying contours.

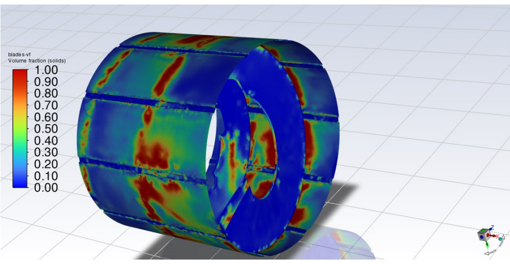

(a) No Rotation.

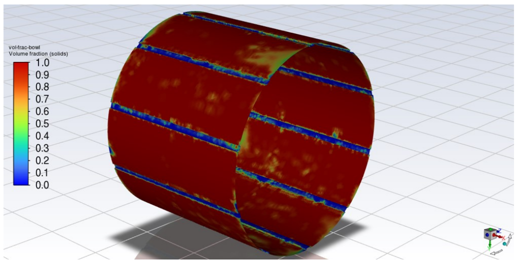

(b) 2.5% of Full Rotation.

Figure 5.4: Analysis of volume fraction of solids along bowl wall.

5.2 Full Decanter

The simulation strategies for the sectioned decanter were mostly carried over for the full decanter. The pressure-based solver along with absolute velocity formulation were the settings used for the solver. A similar approach of starting of with a single phase water case and then applying rotation to the walls of the bowl and conveyor/blades assemblies was used. However, due to instabilities encountered in overall mass conservation, slow ramping up of rotational speed was used in the form of 10% per step for each simulation. Additionally, at different stages of the simulations, both steady state and pseudo transient formulation were used and the first order scheme along with the k-ω turbulence model were used for all simulations. The aims of the analysis were to study the flow fields of both single phase and multiphase cases as well as verify the mass conservation and look into the separation of the solids as well as the direction of flow of both water and solids within the decanter.

For the mass conservation analysis, Figure 5.5 shows the location of the both outlet sides as well as the naming that will be used for the upcoming analysis of the full geometry.

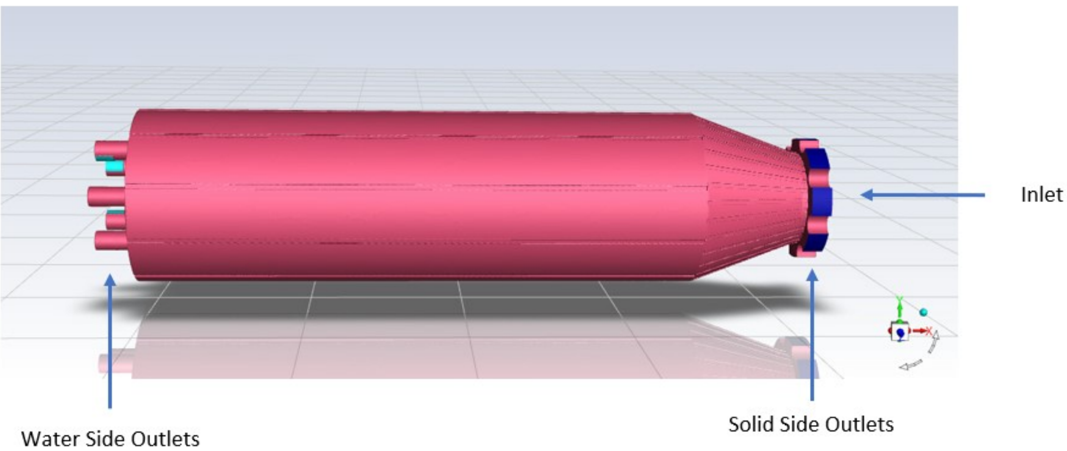

Figure 5.5: Location and naming of outlets for the full decanter.

5.2.1 Single Phase Case

A single phase water case was used to start simulations and test meshes. The aim of the upcoming simulations in this sub section was to extract the needed outlet boundary conditions for multiphase simulations, check mass conservation and check the flow field. Therefore, the key evaluation criterion for these simulation was the stability of the outlet pressure values rather than reaching full convergence.

5.2.1.1 Mass Conservation

The mass conservation was checked for the single phase case. Since the majority of the mixture consist of water, having a stable mass flows at each outlet side would help significantly when the simulations were switched to multiphase by introducing the solids. The rotation was ramped up in steps in order to extract pressure outlet values and use them later on for the multiphase case. Table 5.1 summarizes the mass conservation data for the single phase water case. The negative sign for outlet flow rates indicates flow that exits the computational domain (leaves from outlet surfaces) while a positive value indicates flow entering the computational domain (enters from outlet surfaces). For these simulations, the target mass for each outlet was set within the pressure outlet boundary condition with the values set as 5.7 kg/s for the water side outlet and 1 kg/s for the solid side outlet. The inlet flow is set as 6.7 kg/s.

	Solid Side Outlet	Water Side Outlet	
% of Full Rotation	Mixture Flow Rate (kg/s)	Mixture Flow Rate (kg/s)	Total Accumulation (kg/s)
10	-0.14	-5.46	1.05
40	-1.91	-3.92	4.69
80	6.11	8.49	4.28
Full	1.63	-8.15	0.14

Table 5.1: Mass conservation summary table for the single phase case.

One thing to note that these simulations involved fluctuating flow rates even after stable residuals were reached for both a steady state and a pseudo transit formulation. Thus in many instances, the average flow around a fluctuation point were used as a reference value. The simulation for the 80% rotation was likely not converged but due to time restrictions the rotation was ramped up to full rotation with better convergence reached.

5.2.2 Multiphase Case

For the multiphase simulation, the strategy was to introduce the solids into the decanter through starting from a stable single phase rotation case. Challenges were faced in the form of suitable outlet boundary conditions to use as using atmospheric pressure outlet boundary conditions resulted in large flow rates in each decanter outlet side especially as the rotational speeds were increased. The strategy used involved setting the gauge pressure values from the single phase case for each rotation ramping step as pressure outlet boundary conditions for the multiphase case. A rotational speed of up to 80% of the intended full rotation of the bowl and conveyor/blades was reached with stable and reasonable mass conservation within the domain. Past this rotation speed, the mass flow rates at the outlets resulted in large flow rates again at each outlet.

For these multiphase simulation, a mixture model was used as it provided reasonable stability and computational time. First order upwind scheme was used with a steady-state coupled solver. For rotational speed simulation past 50% of the intended maximum rotation, pesudo transient was used later on in these simulation to reach a stable solution.

5.2.2.1 Mass Conservation

To check the simulations initially, mass flow rate report plots were used to judge the convergence and Table 5.2 shows the mass conservation values for each ramping step for the mutliphase case along with the used outlet pressure boundary conditions. The negative sign for outlet flow rates indicates flow that exits the computational domain (leaves from outlet surfaces) while a positive value indicates flow entering the computational domain (enters from outlet surfaces). The ramping process stages take a significant amount of time to converge to a stable flow rate and thus, for small rotation some of the simulation were run until a stable pressure in the outlet was reached even without a completely stable flow. The inlet flow rate is constant for all cases with a value of 6.7 kg/s for the mixture. Also, early on in the ramping process, some steps were able to be skipped (such as from 10% to 30% rotation).

	Solid Side Outlet		Water Side Outlet		
% of Full Rotation	Mixture Flow Rate (kg/s)	Pressure BC of Outlet (kPa)	Mixture Flow Rate (kg/s)	Pressure BC of Outlet (kPa)	Total Accumulation (kg/s)
10	1.19	-2.1	-7.30	17.8	0.63
30	0.40	29.0	-7.59	186.2	-0.45
40	-0.02	133.2	-7.34	392.4	-0.62
50	3.04	271.9	0.55	661.6	10.3
60	4.63	382.8	1.52	932.7	12.9
70	-3.43	589.8	-3.01	1245.5	0.28
80	-1.41	950.3	-5.20	1832.6	0.12
90	20.47	1284.4	-26.73	2232.4	0.47
Full	9.09	1622.2	-18.5	2783.0	-2.71

Table 5.2: Mass conservation summary table for the mixture model case.

It can be seen that using the pressure outlet values from the single phase case helped in achieving more realistic values as compared to earlier test simulations resulting in flow rates in the region of 150 kg/s leaving each outlet for a full rotation simulation with an atmospheric pressure outlet boundary condition. However, the 90% and full rotation cases provided a noticeable increase and could mean a significantly slower ramping step than 10% would need to be used to reach reasonable values. Therefore, the 80% rotation case was chosen for the upcoming analysis. Furthermore, the results for the 50% and 60% cases show large accumulations but had a stable enough residuals and ramping to the next step did not result in instabilities for the later simulations.

5.2.2.2 Flow Field

As for the flow field within the decanter domain, Figure 5.6 shows the velocity distribution for a cross sectional plane. In Figure 5.6(a), the distribution of the mixture is shown and it can be seen that the velocity magnitude increases from the inlet as it enters the blade helical portion in between the walls of the bowl and the conveyor. The velocity reaches a maximum value of 140.12 m/s and the velocity is at its highest values near the bowl wall as the solids get pushed to the bowl wall. Figure 5.6(b) shows the solids velocity distribution across the same plane and illustrates how the solids move towards the solids side outlet with larger velocities reaching a maximum of 217.71 m/s. The solids direction of flow replicates the decanters' function however, it can be seen that the velocity stops increasing as the flow reaches the conical section which indicates that solids' accumulation is happening within the domain. This will be a point of discussion later on.

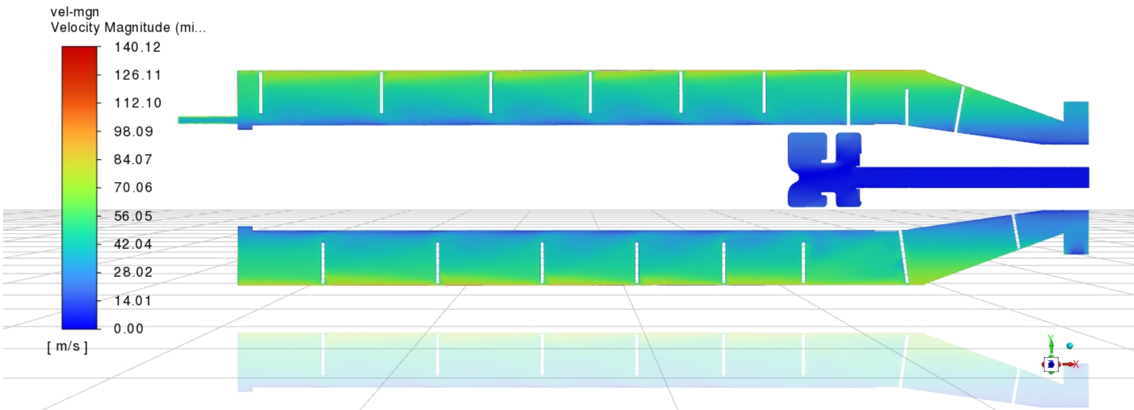

(a) The mixture's velocity magnitude.

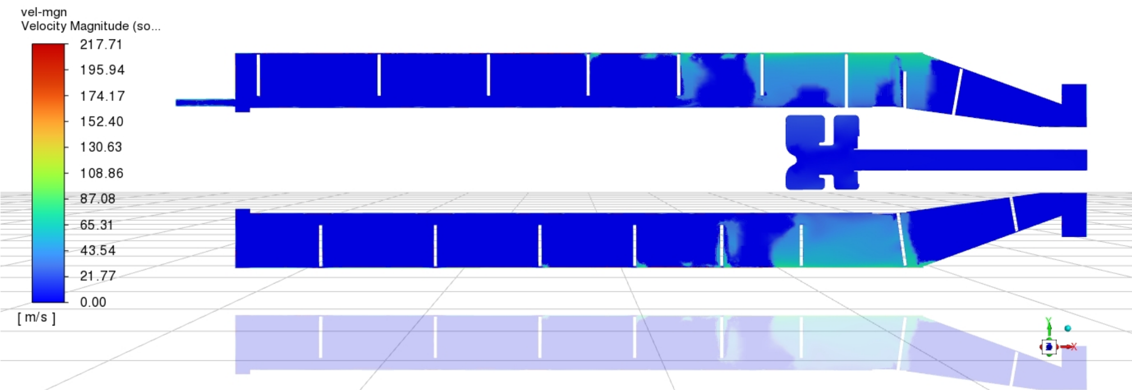

(b) The solids' velocity magnitude.

Figure 5.6: Velocity magnitude for a plane at z=0.

The velocity magnitude for different cut through planes along the x-axis is shown in Figure 5.7. In Figure 5.7(a), the conical part of the bowl is displayed. Within the feed zone shown in Figure 5.7(b), the low velocity seen centrally can be attributed to the axial velocity decreasing as the fluid exits the stationary feed tube. This happens as the flow enters a highly rotating feed zone as the velocity transitions more into the radial direction and as it exits that zone into the helical blade section. Figures 5.7(c) and 5.7(d) show planes further within the symmetrical part of the rest of the domain.

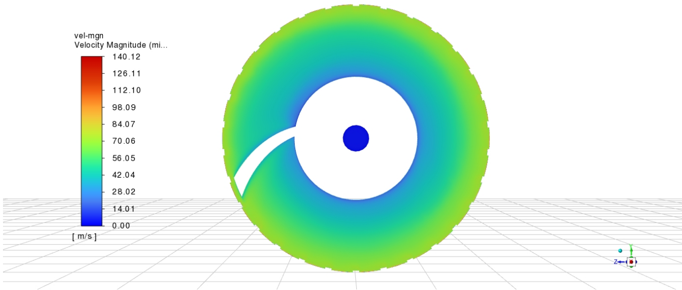

(a) Plane at x≈(5D) mm.

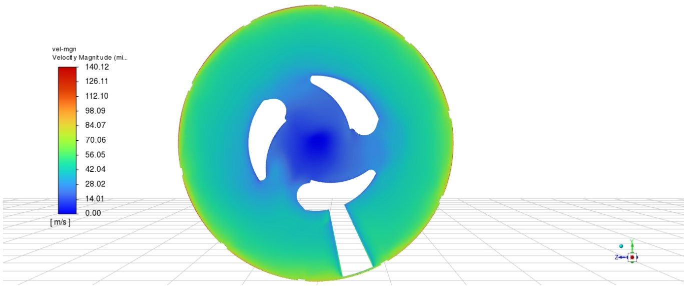

(b) Plane at x≈(16D) mm.

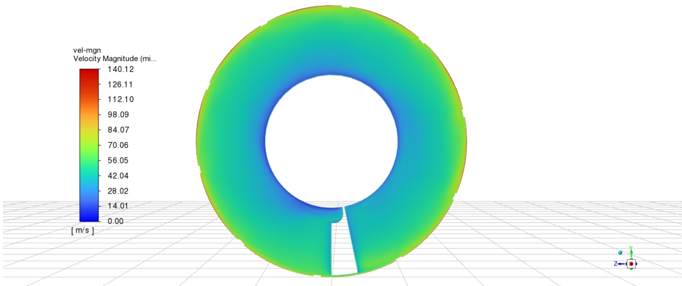

(c) Plane at x≈(35D) mm.

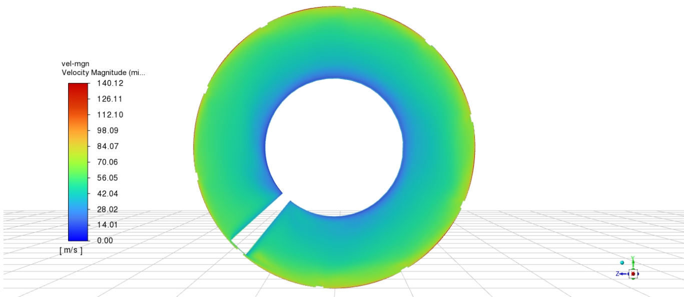

(d) Plane at x≈(52D) mm.

Figure 5.7: Velocity magnitude for planes at different cross sections along the x-axis.

To analyze the centrifugal forces more closely, the axial and radial velocities for a plane in Figure 5.8 are shown. In Figure 5.8(a), the axial velocity indicates how the centrifugal forces are capable of creating the separation phenomena as a higher value of axial velocity indicates higher separation [16]. A positive value for the axial velocity indicates the flow moves towards the solids' outlet side (towards the positive X direction in the axis) while a negative value indicates the flow moves towards the water's outlet side (towards the negative X direction in the axis). The complexity seen with the distribution is likely due to the internal geometry's influence as well as the choice of outlet boundary conditions along with the direction of rotation of both the bowl and conveyor/blades assembly and the differential speed between them. It is important to point out that the limitations present with the mixture model having a combined average velocity for both the water and solids makes it so separating the axial and radial velocities into its water and solids components difficult to analyze for this simulation. Figure 5.8(b) is for the radial velocity for the same plane cut view. Figure 5.9 shows cut through planes of the radial velocity at different points along the x-axis to better show the effect. Focusing on the feed zone as the flow exits the three opening in Figure 5.8(b) it can be seen that the velocity varies significantly in both direction and magnitude within that region due to the large rotational speeds in this simulation. This large variation will influence the separation and can contribute to the turbulence and large velocity at which the mixture is fed through the stationary feed tube [16].

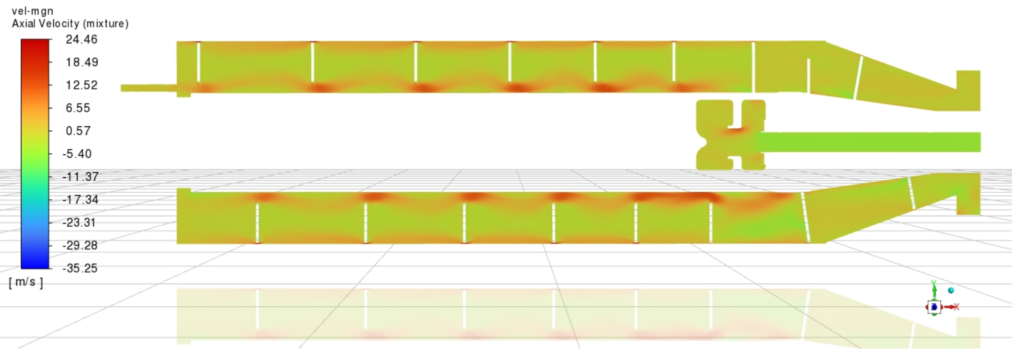

(a) Axial velocity.

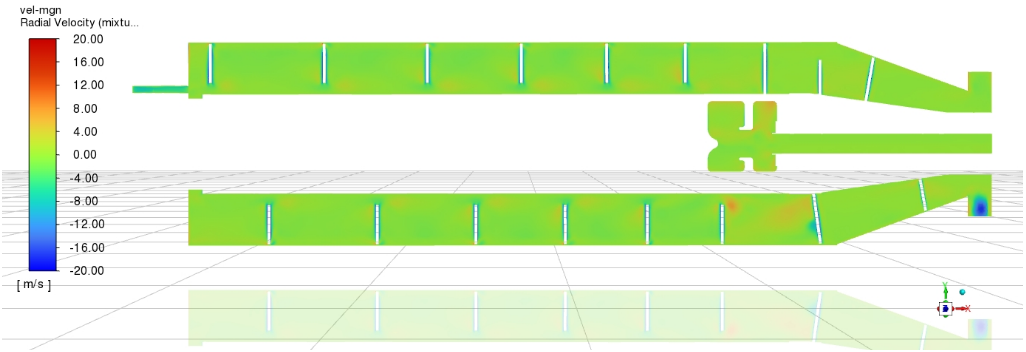

(b) Radial velocity.

Figure 5.8: Axial and Radial velocity for a plane at z=0 for the mixture.

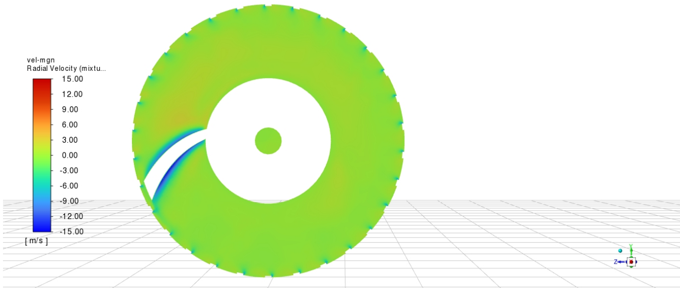

(a) Plane at x≈(5D) mm.

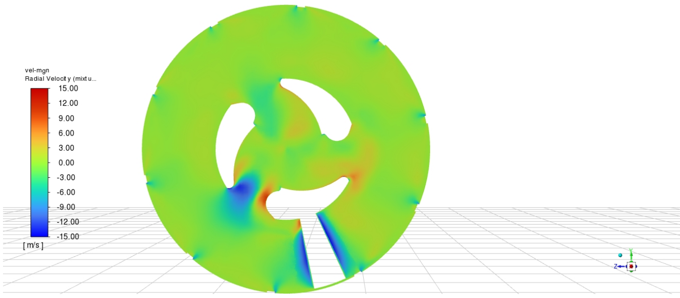

(b) Plane at x≈(16D) mm.

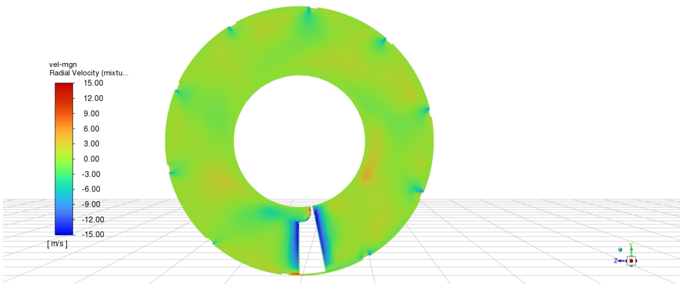

(c) Plane at x≈(35D) mm.

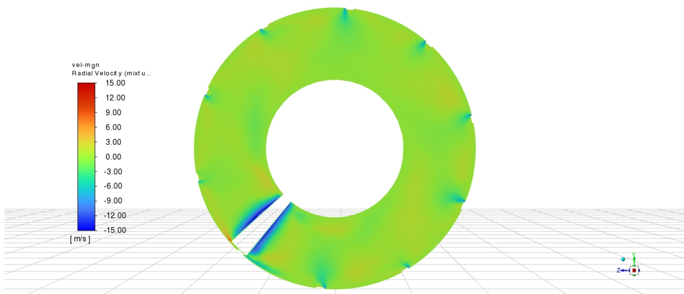

(d) Plane at x≈(52D) mm.

Figure 5.9: Radial velocity magnitude for planes at different cross sections along the x-axis.

Figure 5.10 shows the solids' velocity magnitude at two different locations, the conical part in Figure 5.10(a) and the feed zone in Figure 5.10(b). The solids as predicted by the phenomena move faster at the bowl wall as it travels along the scroll. Within the conical part, the solids seem to have larger velocity in one third of the cross section as it moves along the decreasing diameter in that region towards the solid side outlets. Within the feed zone, the solids exit the three openings into the rotating domain with large velocities as the solids spread across the plane seen here.

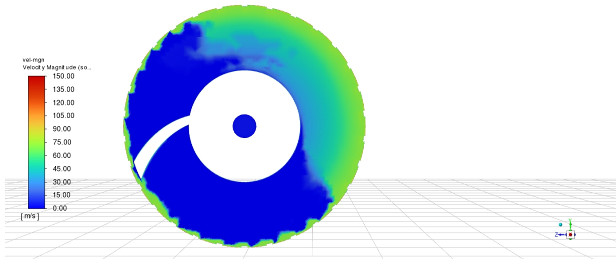

(a) Plane at x≈(5D) mm.

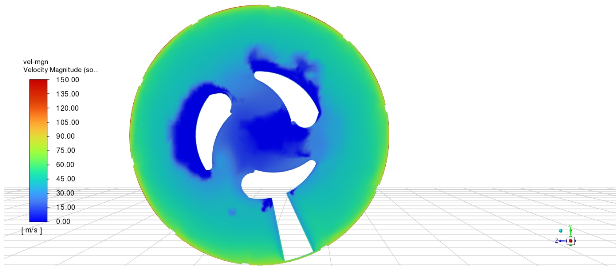

(b) Plane at x≈(16D) mm.

Figure 5.10: Velocity magnitude of solids for planes at different cross sections along the x-axis.

Figure 5.11 shows the pressure distribution within the decanter domain. The highest pressure values occur at the edges of the bowl and lowest in both the inlet tube and towards the solid side outlet region.

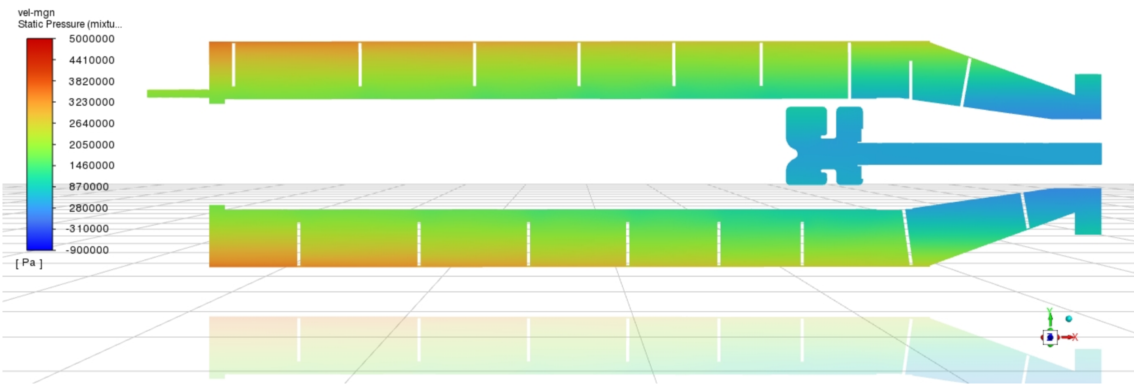

Figure 5.11: Static pressure distribution for a plane at z=0.

5.2.2.3 Separation Efficiency

To analyze the efficiency of separation within the decanter separator, the accumulation of the solids' is discussed . During the rotating multiphase flow simulations, the solids were found to accumulate on the wall as seen in Figure 5.12. This happens in the transition region in between the bowl and the conical section. Therefore, few simulations were conducted for the purposes of analyzing the solids flow direction as well as the amount of solids approaching the conical region. Figure 5.13 displays a modified geometry that consist of the bowl without the conical part that was used for these tests. The aim was to see how the rotational speed's gradual increase effects how much of the solids reach an arbitrary solids outlet surface seen on the positive X-axis direction. Table 5.3 details the solids flow rates at each outlet side for different rotational speeds for an inlet flow of 0.24 kg/s of solids which is equivalent to 3.6% of the total inlet flow.

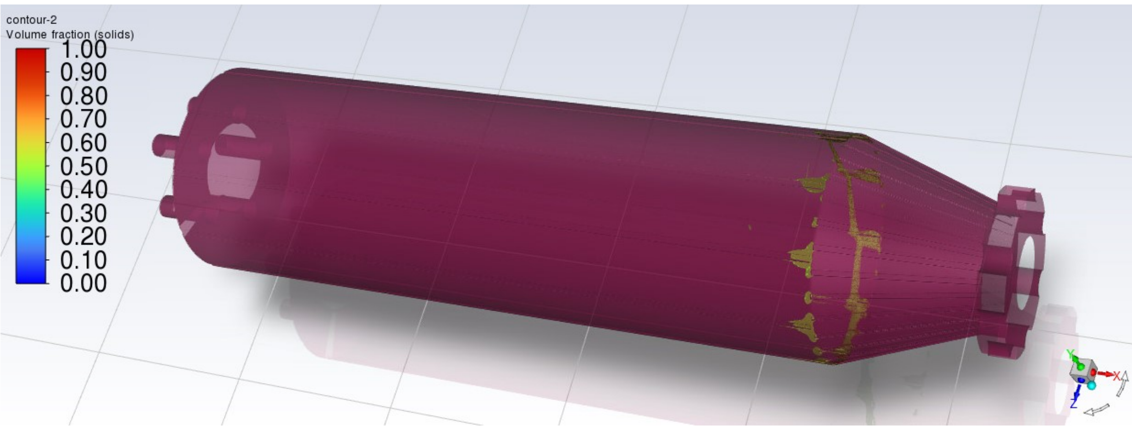

Figure 5.12: Location for the solids accumulation.

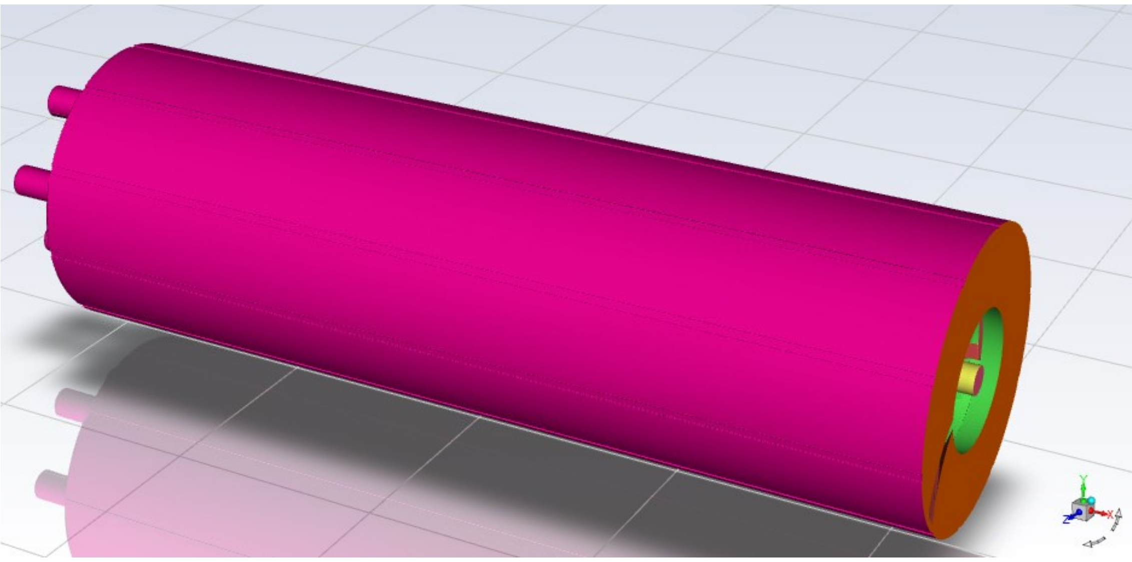

Figure 5.13: Modified Solid Outlet Side.

	Solid Side Outlet	Water Side Outlet	
% of Full Rotation	Solids Flow Rate (kg/s)	Solids Flow Rate (kg/s)	Total Solid Accumulation (kg/s)
20	-0.151	-1.62e^{-7}	0.090
40	-0.179	-5.14e^{-7}	0.062
60	-0.188	-6.03e^{-7}	0.053
80	-0.190	-7.17e^{-7}	0.050
Full	-0.196	-7.91e^{-7}	0.045

Table 5.3: Mass flow rates of solids for test simulations with the adjusted outlet and no conical section.

Figure 5.14 shows the distribution of volume fraction of solids within different positions along the x-axis showing the accumulation happening in positions close to the conical part with the high peaks that are seen.

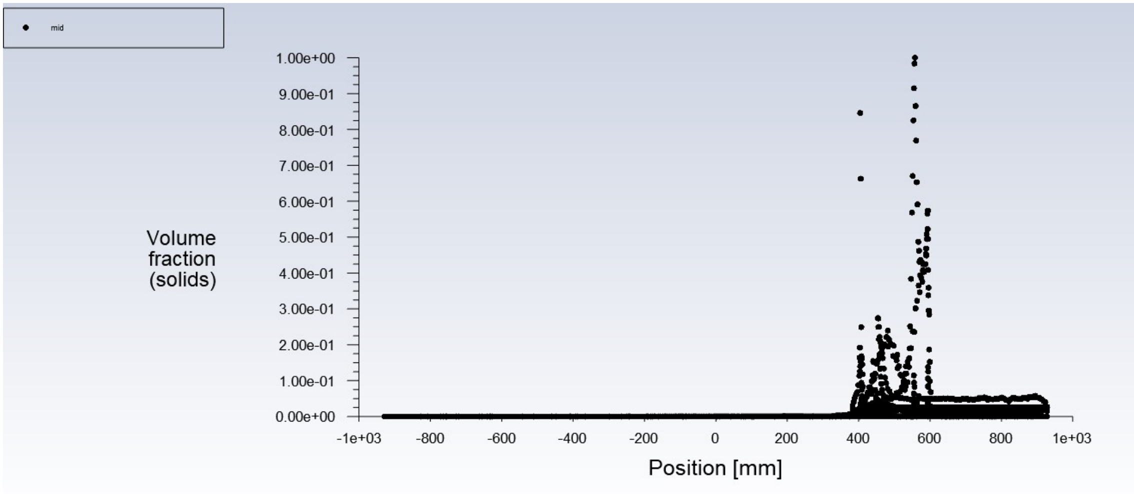

Figure 5.14: Volume fraction of solids for a plane at z=0.

6 Discussion and Conclusions

From the results, it is illustrated that the simulations to some extent capture the key phenomena involved with the decanter separator. However, there are many points of discussion that had a large impact on the results. Here, the most important points from the results will be mentioned.

6.1 Accumulation of Solids

As was seen in Figure 5.12. The solids accumulated in the transition region between the bowl and conical part.The following were done in attempt to fix this:

- **Changed the Orientation of the Bowl:** The bowl was rotated to where the ribs extrusions of the bowl were aligned in a way that allows the flow to transition better.

- **Recombining and Aligning the Geometry:** The geometry of the bowl and the conical region were first combined then were aligned together in SpaceClaim.

The adjustments did not stop the accumulation of solids in that region in subsequent simulations. This could be attributed to these simulation being transient in reality to where a steady state or a pseudo transient formulation was not sufficient to reach convergence.

6.2 Choice of Multiphase Model

The choice of multiphase model can be made based on the Stokes number calculations using Equation 3.12 and Equation 3.15. The choice of the length scale of the system would be the determining factor in the calculations involving the Stokes and the turbulence Stokes numbers. Additionally, looking at the few simulations done as in Figure 5.2, there were slight differences for the sectioned geometry between the mixture model and Euler-Euler model which indicates that limitations with computational time, mesh requirements and solution stability encountered with Euler-Euler made it so the mixture model was used for the full decanter.

6.3 Choice of Outlet Boundary Conditions

Using artificial pressure values for the outlet boundary conditions as shown in Table 5.2 in order to maintain reasonable flow rates for the water in each outlet provided good results in terms of mass conservation for the mixture model. However, comparing to reality, the decanter is operated with open outlets and using values in the ranges shown in the table for the outlets would require sealing the decanter. Furthermore, setting the outlet to such values may create an artificial wall that makes the pressure applied within the domain higher than that set at the outlets in order to transport the flow in the desired direction. This can also help explain the axial velocity distribution present in Figure 5.8. The axial velocity flows for the mixture is seen to be flowing to the left at the edge of the conveyor (through the openings of the blade section seen in Figure 2.6). In reality, the water should travel to left towards the water side outlets through these openings. This is likely caused by using artificial gauge pressure values from the single phase case as boundary conditions.

6.4 Summary

To Conclude:

- Key phenomena involved with the function of the decanter separator were relatively well captured by the simulations.

- Different simulation strategies and models were tested for simulations of the centrifuge decanter separator.

- Accumulation of solids happened between the bowl and conical region of the decanter for the multiphase case.

- An approach with ramping up the rotational speeds of the bowl and conveyor/blades was used with relatively good mass conservation up to a certain value.

- Boundary conditions of the outlets were a key point of discussion and are highly influential for the simulation results.

7 Future Work

7.1 Additional Simulations

Multiphase flow modeling involve a large number of different setting, parameters and models and due to the limited time frame of this project many settings and models have not been investigated. A future study could look into adding other body forces of interest. Additionally, the study of particle-particle interactions is a topic of interest for further investigations and model refinement.

7.2 Mesh Independence

A study involving mesh independence could also be conducted. The aim would be to confirm that mesh size has no affect on the simulation results and would make comparison between different settings more accurate as well as allow the possibility to use meshes of less size in order to save on computational time.

7.3 Rotating Mesh Approach

Fully transit simulations could be used in a further study with the addition of a rotating mesh approach to model the rotation in a more accurate way. The effect of using the moving reference frames approach in this work served to model the rotation in a good way and replicated many of the phenomena present in reality. However, a test with the sliding mesh approach would likely provide more accurate results and serves as a good basis for future simulations.

7.4 Non Inlet Flow Decanter

Lastly, one could also perform a simulation with a decanter that has reached steady state and with no flow coming from the inlet to replicated how in reality, the decanter can be left running with no flow coming into the domain overnight in some instances.

Bibliography

[1] Pang, C., Tan, W., Sha, E., Tao, Y., Liu, L. (2012). Simulating multiphase flow in a two-stage pusher centrifuge using computational fluid dynamics. Frontiers of Chemical Science and Engineering. 6. 329-338.

[2] Liu, Hongbin Li, Pingying Xiao, Huina Mu, Weitao. (2015). The fluid-solid coupling analysis of screw conveyor in drilling fluid centrifuge based on ANSYS. Petroleum. 51.

[3] Shokrian, A., Mobli, H., Akbarnia, A., Jafari, A., Mousazade, H., Zhu, B.L. (2018). Application an Euler–Euler Multiphase-Flow Model for Simulation Flow in a Centrifugal Separator Machine. American Journal of Fluid Dynamics. 8(4). 112-115.

[4] Zhu, M., Hu, D., Xu, Y., amp; Zhao, S. (2019). Design and Computational Fluid Dynamics Analysis of a Three-Phase Decanter Centrifuge for Oil-Water-Solid Separation. Chemical Engineering Technology Special Issue: Particle and Powder Technology. Wiley. 43(5).

[5] Berk, Z. (2009). Food process engineering and technology (1st ed.). International Series. Academic Press Elsevier Inc.

[6] Records, A., Sutherland, K. (2001). Decanter Centrifuge Handbook (1st ed.). Elsevier Advanced Technology.

[7] Bell, G. (2013). Analysis and Development of a Decanter Centrifuge. PhD Thesis. University of Canterbury.

[8] B. Andersson, R. Andersson, L. Håkansson, M. Mortensen, R. Sudiyo, B. van Wachem (2011). Computational Fluid Dynamics for Engineers. Cambridge University Press.

[9] White, John. (2013). CFD Simulation of Silica Gel and Water Adsorbent Beds Used in Adsorption Cooling System. PhD Thesis. University of Birmingham.

[10] ANSYS Fluent Theory Guide (2017), 18th release, ANSYS Inc., Canonsburg, Pennsylvania.

[11] Menter, F. R. (1993), Zonal Two Equation k-ω Turbulence Models for Aerodynamic Flows. AIAA Paper. Eloret Institute. 93-2906.

[12] Zore, K., Shah, S., Stokes, J., Sasanapuri, B., Sharkey, P. (2018). Ansys CFD study for High Lift Aircraft Configurations. 2018 Applied Aerodynamics Conference. American Institute of Aeronautics and Astronautics.

[13] Fontes, E. D. (2020). Modeling and Simulation of Multiphase Flow in COMSOL®: Part 1. COMSOL Multiphysics®.

[14] ANSYS SpaceClaim User,s Guide (2016), ANSYS Inc., Canonsburg, Pennsylvania.

[15] ANSYS Fluent Meshing User Guide (2016), 17th release, ANSYS Inc., Canonsburg, Pennsylvania.

[16] Cheng, Q., Liu, H., Tian, Y. (2016). An Analysis on the Velocity Field of Decanter Centrifuge on the Basis of Fluent. International Journal of Engineering and Advanced Research Technology (IJEART). 2(3).

DEPARTMENT OF CHEMISTRY AND CHEMICAL ENGINEERING
CHALMERS UNIVERSITY OF TECHNOLOGY
Gothenburg, Sweden
www.chalmers.se

CHALMERS
UNIVERSITY OF TECHNOLOGY